Energy & Environmental Science

Accepted Manuscript

ROYAL SOCIETY OF CHEMISTRY

www.rsc.org/ees

Advancements in Perovskite Solar Cells: Photophysics behind the Photovoltaics

Tze Chien Sum[1]* and Nripan Mathews[2,3,4]*

[1]Division of Physics and Applied Physics, School of Physical and Mathematical Sciences, Nanyang Technological University, 21 Nanyang Link, Singapore 637371.

[2]School of Materials Science and Engineering, Nanyang Technological University, Nanyang Avenue, Singapore 639798.

[3]Energy Research Institute @NTU (ERI@N), Research Techno Plaza, X-Frontier Block, Level 5, 50 Nanyang Drive, Singapore 637553.

[4]Singapore-Berkeley Research Initiative for Sustainable Energy, 1 Create Way, Singapore 138602, Singapore.

*Correspondence to: Tzechien@ntu.edu.sg; Nripan@ntu.edu.sg

Abstract

Solution-processed organic-inorganic perovskite solar cells are hailed as the recent major breakthrough in low-cost photovoltaics. Power conversion efficiencies approaching that of crystalline Si solar cells (exceeding 15%) have been reported. Remarkably, such phenomenal performances were achieved in a matter of 5 years – up from ~3.8% back in 2009. Since then, the field has expanded exponentially. In this perspective, we review the basic working mechanisms of perovskite solar cells in relation to their intrinsic properties and fundamental photophysics. The current state-of-the-art and the open questions in this maturing field are also highlighted.

Keywords: Perovskite Solar Cells, Organic-inorganic lead halides; device performance; charge dynamics and photophysics

1. Introduction

Solar power is the world's most abundant energy resource. A year's worth of sunlight contains 1.5 × 10^{18} kWh of energy. By comparison, the known reserves of oil, coal, and gas are 1.75 ×10^{15} kWh, 1.4 ×10^{15}kWh, and 5:5 ×10^{15} kWh, respectively. Thus, a year's worth of sunlight provides more than a hundred times the energy of the world's entire known fossil fuel reserves. Harnessing solar power would yield a never-ending energy supply.[1] The difficulty has always been converting solar energy in an efficient and cost-effective way. Photovoltaic cells are the most promising avenue, directly converting the photons to electricity. For photovoltaic energy to become competitive with fossil fuels and capture a significant share of the electricity market, it is necessary to reduce the total cost of solar energy. This can be achieved by either reducing the cost of photovoltaic cells or by increasing their power conversion efficiency.

The photovoltaic market is currently dominated by crystalline Si solar cells with efficiencies close to 20%. Alternative "third generation" technologies such as organic photovoltaics (OPVs), dye sensitized solar cells (DSCs) and quantum dot solar cells (QDSCs) which are fabricated through solution based processes such as blade coating, screen printing and spraying, promise low cost solar power while allowing the utilization of unconventional substrates. Although the utilization of low temperature processes reduces the energetic costs and the energy payback time, the power conversion efficiencies (PCEs) of these solar cells still lag significantly behind conventional solar cells. The levelized cost of energy (LCOE) which allows for the comparison of various electricity generation sources, depends critically on the efficiency of the solar cells produced.[2] A more efficient module yields more power per unit area. A significant fraction of a solar cell's cost scales proportional to the installation area, including the cost of the glass, inverter costs and installation costs, among others. A more efficient solar cell allows for a reduction in all the costs associated with installation, while requiring much lower numbers of solar panels to be installed. Thus power conversion efficiency is a primary driver of cost for solar cells.

Organic-inorganic halide perovskite solar cells has been the most significant development in the field of photovoltaics in the present decade and is the best bet at satisfying the need for high efficiencies while allowing for low cost solution based manufacturing. Since the first reports of stable solid state solar cells based on $CH_3NH_3PbI_3$ perovskite in mid-2012, the PCEs of the solar cells have already exceeded 15%, leapfrogging every other solution-processed solar cell technology. The wide range of efficient perovskite solar cell device architectures demonstrated point towards a remarkable semiconducting material with excellent electrical and optical properties. Early pioneering work[3, 4] in the area of organic-inorganic halides has clearly shown that this class of materials can behave as low dimensional electronic

systems with tunable properties, allowing for the development of newer perovskite solar materials in addition to $CH_3NH_3PbI_3$.

This review focuses on the recent developments (*i.e.*, up to Feb 2014) in perovskite solar cells as well as their photophysical properties and charge dynamics. We first review the intrinsic physical and electronic properties of this class of organic-inorganic perovskites, followed by its progress as a photovoltaic material. The review then examines the recent photophysical studies on unraveling the charge dynamics and transport mechanisms in both perovskite thin films as well as in perovskite solar cells. Due to the rapid pace of research in this area, this review does not aim to be comprehensive but will highlight key work and findings. Lastly, we conclude the review with the open questions facing these classes of solar cells and future directions of research.

2. Intrinsic Properties of Organic-Inorganic Perovskites

(a) Physical Structure

Perovskites is a common nomenclature for compounds with the generic chemical formula of AMX_3. In the cubic unit cell, the A-cation resides at the eight corners of the cube, while the M-cation is located at the body center that is surrounded by 6 X-anions (located at the face centers) in an octahedral $[MX_6]^{4-}$ cluster. Typical inorganic perovskites include $CaTiO_3$ and $SrTiO_3$. Due to the interplay of the charge, spin and structural properties, this family of materials is known to exhibit a plethora of novel and exciting phenomena such as superconductivity, magnetoresistance, ferroelectricity, magnetoelectricity, anti-ferromagnetism, anti-ferroelectricity *etc*.[5] In the classes of compounds being discussed here, the A cations are organic (typically $CH_3NH_3^+$,$C_2H_5NH_3^+$, $HC(NH_2)_2^+$), the metal cations (M) are typically divalent metal ions such as Pb^{2+}, Sn^{2+}, Eu^{2+}, Cu^{2+} etc, while the X anions are halides (Cl^-, Br^-, I^-). $CH_3NH_3PbI_3$ belongs to a large family of organic-inorganic perovskites where the $[PbI_6]^{4-}$ octahedral can form 3-D, two-dimensional (2-D), one-dimensional (1-D) or zero-dimensional (0-D) networks, possessing the same unit structure – Figure 1. The absence of any inhomogenous broadening (arising from size distribution of the samples) in these 3-D and their low-dimensional counterparts makes these compounds ideal for investigating quantum confinement effects in semiconductor mesoscopic structures. Pioneering work in this class of compounds began as early as 1989 where the focus was on the effects of dimensionality on the excitonic, optical and electronic properties.[4, 6, 7] The optoelectronic properties of layered organic-inorganic perovskites were also extensively studied because of the novel properties exhibited by these crystals which include: high mobilities for thin-film transistors[8, 9]; strong excitonic

properties for light emitting diodes[10, 11]; large nonlinearities with ultrafast response[12, 13]; and even polariton emission in 2D perovskite-based microcavities.[14-18]

In $CH_3NH_3PbI_3$, each $[PbI_6]^{4-}$ octahedron is connected with six neighbours at the iodide – forming a 3-D network. The countercation ($CH_3NH_3^+$) is located at the void of the network. For the 2-D case[19] (*e.g.*, $(CH_3NH_3)_2PbI_4$, each $[PbI_6]^{4-}$ octahedron is connected with four neighbours at the halide – forming a 2-D network layer that is sandwiched between two $CH_3NH_3^+$ layers (also not shown in figure). A multiple quantum well structure results with the stacking of these sandwiched layers via van der Waals interaction – with the 2-D $[PbI_6]^{4-}$ functioning as the quantum well and the $CH_3NH_3^+$ layer as the barrier. For the 1-D case[20] (*e.g.*, $(NH_2C(I) = NH_2)_3PbI_5$), each octahedron is connected at two opposite corners with its neighbour – forming separate infinite chains. Lastly, the quantum dot (0-D) analogue manifests as $(CH_3NH_3)_4PbI_6.2H_2O$, where each $[PbI_6]^{4-}$ complex is neutralized by four $CH_3NH_3^+$ ions to form a molecule. A quantum dot array results when these molecules are isolated by H_2O molecules to form a molecular crystal.

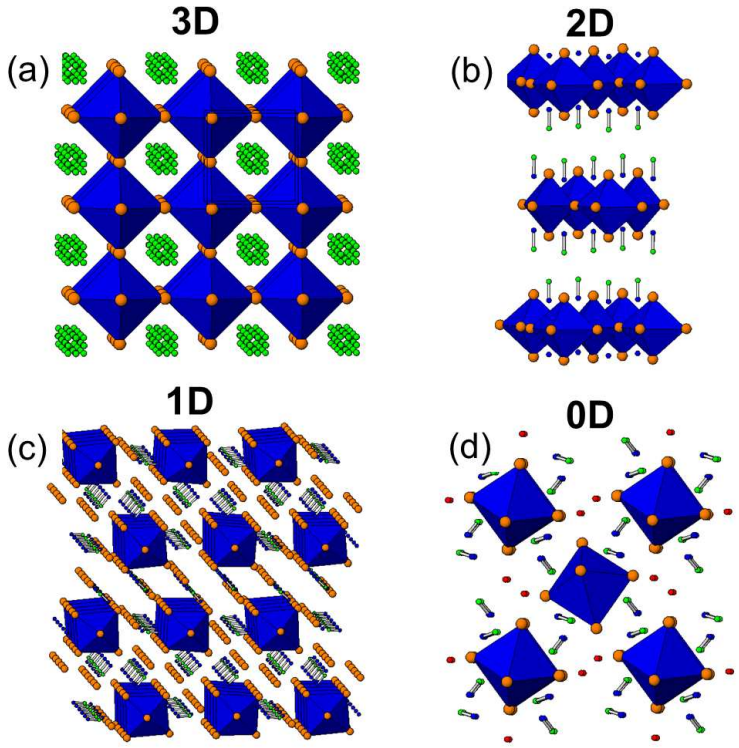

Figure 1: Crystal Structures of (a) $CH_3NH_3PbI_3$,[21] (b) $(CH_3NH_3)_2PbI_4$,[19] (c) $(C_{10}H_{21}NH_3)_2PbI_4$,[20] and (d) $(CH_3NH_3)_4PbI_6.2H_2O$,[22] corresponding to 3D, 2D, 1D and 0D networks. The blue polyhedra represent the MX_6 (M = Pb, Sn and Cu; X = I and Br) octahedra with the halogens represented by orange spheres – the building block of these compounds. The blue, green and red spheres are the N, C and O respectively (the H ions were removed for clarity). The ID network extends into the plane of the document.

(b) Electronic Structure

Early studies on the electronic band structures of organic-inorganic (3-D and low-dimensional) perovskites can be traced to the works by: Koutselas *et. al.* [7] using band structure calculations by a semi-empirical method based on the extended Hückel theory and an *ab-initio* approach based on the Hartree-Fock theory; T. Umebayashi *et. al.*[23] using ultraviolet photoelectron spectroscopy and first principles density functional theory (DFT) band calculations for the room temperature cubic phase; and Chang *et. al.*[24] using first principles pseudopotential calculations. DFT calculations for the 3-D $CH_3NH_3PbI_3$ crystal revealed that the valence band maxima comprises the Pb 6p – I 5p σ-antibonding orbital, while the conduction band minima consists of Pb 6p – I 5s σ anti-bonding and Pb 6p – I 5p π anti-bonding orbitals (See Figure 2 below).[23]

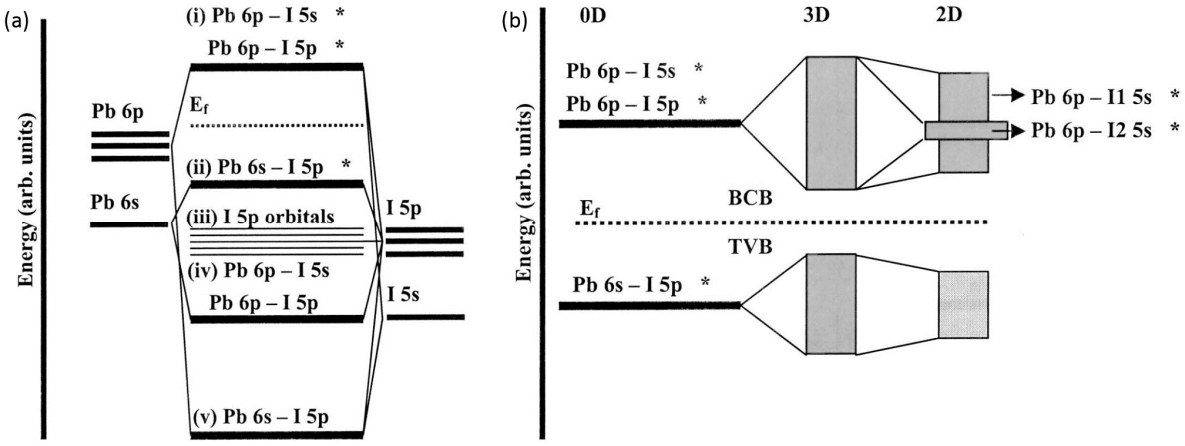

Figure 2: Bonding diagram of (a) $[PbI_6]^{4-}$ cluster (0-D), (b) $CH_3NH_3PbI_3$ (3-D) and (b) $(C_4H_9NH_3)_2PbI_4$ (2-D) at the top of the valence band and the bottom of the conduction band. Reproduced with permission from ref. 23 copyright 2003, American Physical Society (APS).

Following the attention garnered by perovskite solar cells, renewed interests in the DFT studies of 3-D perovskites began in earnest with the work of E. Mosconi together with F. De Angelis and their collaborators.[25] They calculated the band structure for $CH_3NH_3PbX_3$ (cubic phase) and the mixed halide $CH_3NH_3PbI_2X$ (tetragonal phase) (X = Cl, Br and I) with the surrounding $CH_3NH_3^+$ counterions, which were ignored in the earlier studies. Nevertheless, the organic component had little influence to the bandgap energy, of which is mainly determined by the $[PbI_4]^{6-}$ network. In addition, the authors highlight that the close matching of their calculated bandgaps (where spin-orbit coupling (SOC) effect were not considered) with the experimental data is likely to be fortuitous. These findings are consistent with those in the later works by T. Baikie *et. al.*[26] and Y. Wang *et. al.* (low-temperature orthorhombic phase)[27]

Investigation on the SOC effect on the electronic band structure in 3-D perovskites (low-temperature orthorhombic phase) was reported by J. Even *et. al.*[28], where they found that the SOC dramatically reduces the energy gap affecting mainly the conduction band.

Having covered the fundamental properties of the large family of organic-inorganic perovskites, we next focus our attention on $CH_3NH_3PbI_3$ and their photovoltaic applications.

3. Progress in Perovskite Photovoltaics

Initial studies in the area of perovskite solar cells arose as an evolution of the dye sensitized solar cell[29] architecture. DSCs typically consist of a mesoporous n-type TiO_2 electrode which has been sensitized by a dye and placed in a liquid electrolyte (typically I^-/I_3^- redox couple). Since the grafted dyes only form a monolayer, the mesoporous electrode must be 10-15 μm thick to enable complete light absorption. The development of alternative semiconducting sensitizers (either in thin film or QD form) allows for a reduction in the mesoporous TiO_2 layer thickness. Miyasaka and coworkers[30] in 2009 demonstrated the first perovskite sensitized solar cells utilizing $CH_3NH_3PbI_3$ and $CH_3NH_3PbBr_3$ as light absorbers on TiO_2 mesoporous layers with halide electrolytes. A significant efficiency of 3.81% was obtained from $CH_3NH_3PbI_3$ with photocurrent onset observed from ~800 nm. An impressive photovoltage of 0.96V was obtained from $CH_3NH_3PbBr_3$, attributed to the deeper bromide redox couple used in such solar cells. Further improvements[31] in such liquid electrolyte solar cells were made by N.G. Park and coworkers in 2011 through a careful optimization of the mesoporous layer thickness, perovskite concentration and surface treatment. Surface modification of TiO_2 with $Pb(NO_3)_2$ prior to deposition of perovskite resulted in an efficiency of 6.54% (J_{SC} = 15.82 $mAcm^{-2}$, V_{OC} = 0.706 V and FF = 0.586). Despite the efficiencies achieved in such configurations, the overall instability of the solar cells due to the dissolution of the perovskite in the liquid electrolyte appeared to be a challenge.

A breakthrough in both efficiency and stability was achieved in 2012 through utilization of a solid-state hole transporter 2,2′,7,7′-tetrakis(N,N-p-dimethoxy-phenylamino)-9,9′-spirobifluorene (spiro-OMeTAD) with $CH_3NH_3PbI_3$ and $CH_3NH_3PbI_{3-x}Cl_x$ light absorbers (Figure 3). [32, 33] N.G. Park, M. Grätzel and coworkers reported a PCE of 9.7% (J_{SC} = 17.6 $mAcm^{-2}$, V_{OC} = 0.888 V and FF = 0.62) for $CH_3NH_3PbI_3$ on 0.6μm TiO_2 layers. The use of spiro-OMeTAD dramatically improved the device stability compared to liquid junction cells with ex-situ long-term stability tests for over 500 h, where the devices are stored in air at room temperature without encapsulation.[32] H. Snaith and coworkers on the other hand utilized a mixed halide system - $CH_3NH_3PbI_{3-x}Cl_x$ on both TiO_2 and Al_2O_3 mesoporous layers.

Incredibly, the highest efficiencies (PCE = 10.9%, J_{SC} = 17.8 mAcm^{-2}, V_{OC} = 0.98 V and FF = 0.63) were obtained for the mesoporous Al_2O_3 devices where its acts purely as a scaffold and does not take part in the electrical processes.[33] These two reports sparked an explosion of research activities where a variety of device configurations, deposition protocols and material sets have been employed.

(a) Device Architectures

A common device configuration for $CH_3NH_3PbI_3$ based solar cells consists of infiltrating the perovskite within an n-type mesoporous layer (Figure 3(a)). The solar cell fabrication process commences with the deposition of a compact TiO_2 hole-blocking layer on top of the fluorine doped tin oxide (FTO) substrate. This is typically done through the spray pyrolysis of precursors such as titanium diisopropoxide bis(acetylacetonate) at ~450^{o}C. It is important to ensure that the compact layer is pinhole-free and uniform to prevent the recombination between carriers from the perovskite layers and FTO. On top of the compact layer, a mesoporous layer of n-type TiO_2 is formed either by screen printing or spincoating a nanoparticle TiO_2 paste followed by annealing to remove the polymeric binders. Thickness and porosity of these layers can be modulated by changing the filler and solvent concentrations in the TiO_2 paste. The perovskite films are then deposited on top of the n-type mesoporous layer by spincoating it from a solvent such as γ-butyrolactone (GBL) or N,N-dimethylformamide (DMF). This is followed by the deposition of a hole transporting material (HTM) such as spiro-OMeTAD with appropriate dopants to improve conductivity. Finally, a metal electrode is deposited on top of the HTM to complete the solar cell.

Although TiO_2 nanoparticles are most commonly used,[32, 34-37] there have also been reports of solar cells employing TiO_2 nanosheets[38], nanorods[39], nanofibers[40] as well as other n-type materials such as ZnO.[41, 42] Despite the wide variety of mesoporous architectures being employed, there has been no clear evidence that the efficiencies of the perovskite solar cells can be effectively increased by mesoporous layer modification. The most significant effect of the mesoporous layer that has been noted is how their thicknesses can affect the power conversion efficiencies. Both in the liquid junction configuration, as well as in its solid state equivalent, it has been demonstrated that lower mesoporous layer thicknesses perform better.[31, 32, 39] The highest efficiencies in these kinds of configurations have been obtained with a 350 nm thick mesoporous TiO_2 layer infiltrated with $CH_3NH_3PbI_3$.[35] The high efficiencies of these solar cells at relatively low TiO_2 thicknesses (in contrast to ~3um thickness for solid state DSCs[43] and 10-15 μm thickness for DSCs[44]) can be traced to the high optical absorption coefficient (~10^5 cm^{-1}) of $CH_3NH_3PbI_3$.[31, 45, 46] The exact dependence of the mesoporous layer thickness on the power conversion efficiency is determined by the nature of the perovskite distribution within the TiO_2 layers[47] as well as the perovskite overlayer thickness[34] (which is in turn dependent on the perovskite solution concentration).The

demonstration of good efficiencies[39] in rutile TiO_2 nanowires which have been shown to perform poorly in DSCs (due to poor electron transport)[48], again indicates that the thickness of the mesoporous layer is a more critical factor. An interesting change in this device configuration stems from the work of Etgar and coworkers who have demonstrated that such mesoporous TiO_2 based solar cells do not require a HTM to function.[38, 49] The initial study employed anatase TiO_2 nanosheets as the mesoporous layer[38], onto which the perovskite layers were spuncoated and followed by the evaporation of a gold electrode. The solar cells so fabricated, displayed an efficiency of 5.5% (J_{SC} =16.1 $mAcm^{-2}$, V_{OC}= 0.63 V and FF= 0.57). Further optimization of the perovskite layer thickness through consecutive spincoating resulted in an efficiency of 8%.[49] The successful functioning of such devices indicate that $CH_3NH_3PbI_3$ can act as an effective hole transporter. However, the V_{OC}s of such devices are lower than that produced with spiro-OMeTAD indicating that the lack of electron selection layer results in increased recombination.

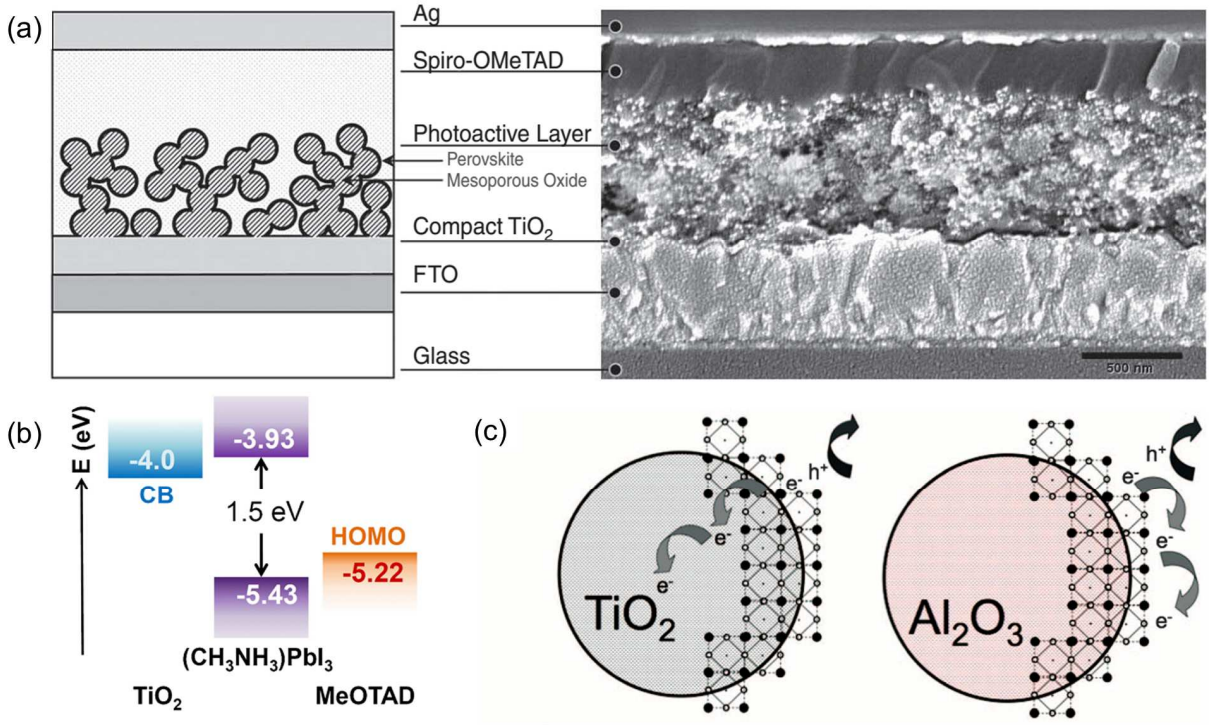

Figure 3: (a) Schematic illustrating mesoporous perovskite solar cells. The mesoporous oxide can be an electron transporting semiconductor such as TiO_2 , ZnO or an insulating layer such as Al_2O_3 or ZrO_2 (meso-superstructured solar cell –MSSC) (b) Relevant energy levels in the mesoporous TiO_2 perovskite solar cells (c) Schematic illustrating the charge transfer and charge transport in a perovskite TiO_2 solar cell and a non-injecting Al_2O_3 based solar cell (a) and (c) are reproduced from ref. 33 copyright 2012, Science (AAAS) and (b) is reproduced from ref. 32 copyright 2012, Nature Publishing Group.

Another efficient solar cell configuration that has been chiefly employed by Snaith and coworkers is the meso-superstructured solar cell (MSSC). This device configuration employs an insulating

mesoporous layer on top of the compact TiO_2 layer as a scaffold to load the perovskite within them. Much of the reports employing this configuration utilize Al_2O_3 as the mesoporous layer and the mixed perovskite $CH_3NH_3PbI_{3-x}Cl_x$ as the absorber.[33, 50-52]

However, the high efficiencies observed in this device configuration are not specific to this material combination. Hagfeldt and coworkers have also demonstrated efficient solar cells (PCE= 10.8%, J_{SC} =17.3 mAcm^{-2}, V_{OC}= 1.07 V and FF= 0.59) by employing $CH_3NH_3PbI_3$ deposited on an insulating ZrO_2 mesoporous layer[36]. The lack of an n-type mesoporous layer in this device configuration clearly indicates that efficient electron transport occurs within the perovskite itself (Figure 3 (c)). This also indicates that the perovskite within the mesoporous layer is continuous, in contrast to previous studies which had considered them as isolated quantum dots.[30, 31] The contrast between both the views could be explained by a recent work[47] which indicated that $CH_3NH_3PbI_3$ exists as two components within the mesoporous TiO_2 , one component with medium range crystalline order (30 atom %) and another with only local structural coherence (70 atom %). The electron transporting nature of the perovskite is further highlighted in the work of Ball et.al.[50] By thinning down the Al_2O_3 scaffold thickness (Figure 4(a)), the authors were able to form solar cells which appeared more as thin film solar cells. The J_{SC} for such solar cells were 16.9±1.9 mAcm^{-2} for thin alumina scaffold layers (80 nm) indicating that thick perovskite films could generate sufficient photocurrent. The ability of the perovskites to be employed in such an electron transporter-free configuration, as well as to perform efficiently in an HTM-free configuration[38, 49], points towards the ambipolar nature of transport in them. However, it is important to note that the MSSCs do not have the reduced V_{OC}s associated with the HTM-free solar cells primarily due to the presence of the hole selective contacts. The effects of carrier accumulation within the perovskite could also be a possible reason for the enhanced V_{OC}s.

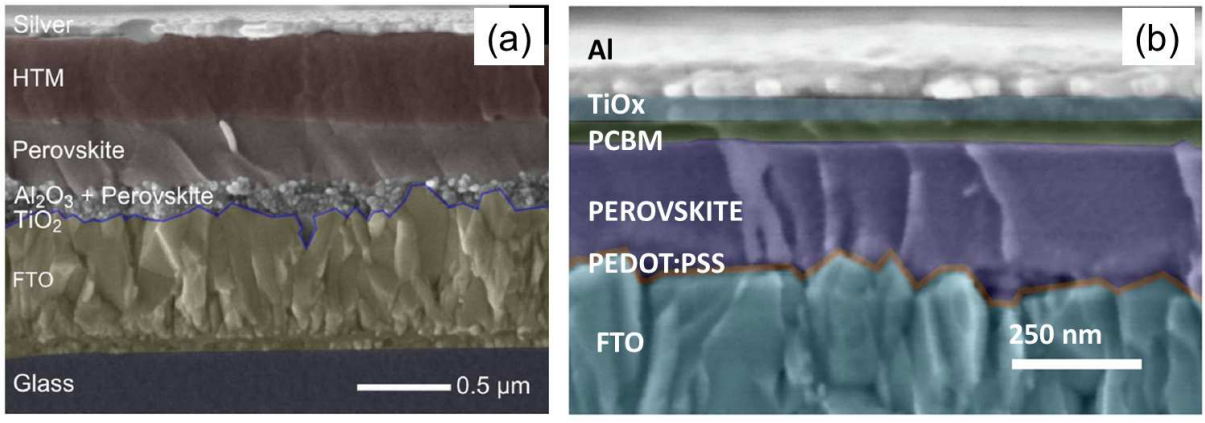

Figure 4: (a) Cross-sectional SEM view of a "pseudo-thin film" architecture employing a thin Al_2O_3 mesoporous layer with a significantly thick perovskite film over it (b) Cross-sectional view of a planar perovskite solar cell

illustrating the typical organic charge transport layers employed. (a) is reproduced from ref. 50 copyright 2013, Royal Society of Chemistry. (b) is reproduced from ref. [53]copyright 2013, Nature Publishing Group.

The success of the "pseudo-thin film" MSSC solar cells drove explorations into planar thin film configurations of the perovskite solar cells. Thin film solar cells allow for a simpler processing route. One approach to realizing such thin film solar cells is to avoid the use of any mesoporous layer and deposit the films directly on the TiO_2 compact layer. The initial report on MSSC had included results from a planar configuration (FTO /compact TiO_2 / $CH_3NH_3PbI_{3-x}Cl_x$ / spiro-OMeTAD / Ag), but with a relatively low efficiency of 1.8%.[33] The difficulties associated with the fabrication of a thin film solar cell stem from the challenges of depositing a homogenous pin-hole free perovskite layer through solution based processes. Poor coverage results in poor light absorption as well as shunting paths through the light absorber layer which reduces efficiency. Unlike polymeric films which are mostly amorphous when deposited by spincoating, the perovskites are crystalline. Even mild heating to remove solvent residues can result in dewetting and roughening of the as deposited perovskite film. Eperon et.al. have carefully studied the morphological effects of the underlying substrate, annealing time, temperature and initial perovskite($CH_3NH_3PbI_{3-x}Cl_x$) film thickness. Through a control of the various factors involved, the authors have achieved an efficiency of 11.4% (J_{SC} =20.3 $mAcm^{-2}$, V_{OC}= 0.89 V and FF= 0.64).[54] A much simpler approach[55] involved the vapour deposition of the perovskite films onto the TiO_2 films which yielded a short-circuit photocurrent of 21.5 mA cm^{-2}, an open-circuit voltage of 1.07 V and a fill factor of 0.68, and an efficiency of 15.4%. An interesting vapor assisted approach to form efficient planar solar cells has also been demonstrated by Yang Yang and coworkers.[56] A 350 nm thick $CH_3NH_3PbI_3$ film formed on the compact TiO_2 layer, yielded an efficiency of 12.1%, despite the relatively thick HTM layer employed in the devices. A similar planar solar cell approach, but which allows for low temperature processing involves the utilization of ZnO as the blocking layer. The first approach by Kumar et.al employed electrodeposited ZnO on both rigid FTO and flexible ITO on top of which $CH_3NH_3PbI_3$ was spuncoated.[41] The second approach utilized spuncoated films from a solution of 5nm ZnO nanoparticles suspended in a butanol/chloroform mixture requiring no calcination or sintering. The authors argue that the lack of a constricting mesoporous layer allows for unconstrained $CH_3NH_3PbI_3$ perovskite crystal growth yielding an impressive efficiency of 15.7% on FTO and 10.2% on flexible ITO substrates.[57]

Another growing area of research involves the use of electron and hole transport layers commonly utilized by the organic photovoltaic community in the implementation of the planar solar cell configuration. The first work in this direction was performed by Chen and coworkers who employed a device architecture consisting of poly(3,4-ethylenedioxythiophene):poly(styrenesulfonic acid) (PEDOT:PSS) as the hole transport layer and C_{60} derivatives including (6,6)-phenyl C61-butyric acid

methyl ester (PCBM) and indene-C_{60} bisadduct (ICBA) as the electron transporter in a planar configuration.[58] As with forming perovskite on top of TiO_2 thin films, the authors faced challenges in forming a uniform $CH_3NH_3PbI_3$ coating on top of the PEDOT:PSS layer. This restricted the total thickness of the $CH_3NH_3PbI_3$ utilized, hence limiting the efficiencies to 3.9%. Sun et.al employed a similar device configuration but succeeded in making a thicker $CH_3NH_3PbI_3$ (110 ± 5 nm) film through the utilization of a two-step conversion approach. The highest efficiency reported in such a device was 7.41%. [45] Snaith and coworkers[53] screened a wider material set employed in OPVs, including NiO and V_2O_5 hole transport layers and poly[(9,9-bis(30-(N,N-dimethylamino)propyl)-2,7-fluorene)-alt-2,7-(9,9–dioctylfluorene)] (PFN) as an electron selective contact with $CH_3NH_3Pb1_{3-x}Cl_x$. However, the most efficient device configuration still employed $PC_{61}BM$ and PEDOT:PSS as the two previous reports covered above. A ~300 nm thick $CH_3NH_3Pb1_{3-x}Cl_x$ layer (Figure 4(b)), yielded an efficiency of 9.8% while flexible solar cells were also fabricated on ITO coated glass yielding 6.3%. Crucially, the lower efficiencies on the flexible devices were attributed to the smoother surface of the ITO layer which affects the uniformity of the perovskite coating. However, even higher efficiencies have been demonstrated for flexible $CH_3NH_3Pb1_{3-x}Cl_x$ solar cells on ITO by Yang Yang and coworkers (9.2%).[59]

(b) Deposition Processes

Much of the initial work on $CH_3NH_3PbI_3$ and $CH_3NH_3PbI_{3-x}Cl_x$ solar cells utilized spin-coating to deposit the light absorbers from a single precursor solution. $CH_3NH_3PbI_3$ films were formed by dissolving stoichiometric quantities of CH_3NH_3I and PbI_2 in polar solvents such as GBL or DMF.[32, 34] $CH_3NH_3PbI_{3-x}Cl_x$ is typically formed from a solution in DMF where the $PbCl_2$ and CH_3NH_3I are in a molar ratio of 1:3.[33, 50] With appropriate optimization of the precursor concentration and spincoating conditions, the perovskite can be deposited within the pores of the mesoporous layers or be used to form compact layers for planar solar cells. As described previously, the formation of a uniform perovskite layer for planar devices through spincoating requires the optimization of multiple parameters including post deposition processes.[45, 54, 58] Due to wettability differences, the perovskite would need to be separately optimized for each underlying layer. When spincoating on mesoporous layers, conditions similar to the deposition of HTMs within the mesoporous TiO_2 layers of a solid state DSC could be expected to occur.[60] In such a case, the excess solution on top of the film can act as a reservoir during the spincoating process. The amount of infiltration within the mesoporous layer could deposit critically on solution concentration, spincoating speed and the solvent utilized. The tendency of the perovskite films to crystallise, could lead to rough surface morphologies[34] which could introduce shunts into the solar cells.

A significant development for solution based deposition has been the application of the sequential deposition process (originally developed by Mitzi and coworkers[61]) to the fabrication of perovskite solar cells by Grätzel and coworkers.[35] The process consists of first spincoating PbI_2 on the TiO_2 layer from a solution with concentrations and spincoating speed set to enable infiltration within the mesoporous layer (Figure 5(a)). Subsequently, the yellow substrates are dipped in a $CH_3NH_3PbI_3$ solution in 2-propanol solvent. During the dipping, the yellow PbI_2 converts to form the dark brown $CH_3NH_3PbI_3$ in a few seconds (Figure 5(b)). It is important to note that the conversion time can vary between the different PbI_2 conditions. A 20 minute conversion time has been reported for perovskite solar cells[40], while the initial work by Mitzi and coworkers indicated that the conversion required 1-3h[61]. It is likely that the PbI_2 layer deposited on top of mesoporous substrates has increased roughness that allows the conversion reaction to proceed faster.[35] Due to the volume expansion[56] (~75%) occurring due to the conversion of PbI_2 into $CH_3NH_3PbI_3$, it can be expected that the mesoporous layer would be better infiltrated through the sequential deposition process. The top view of the sequentially deposited samples reveals a highly crystalline film with complete coverage (Figure 5(c)).

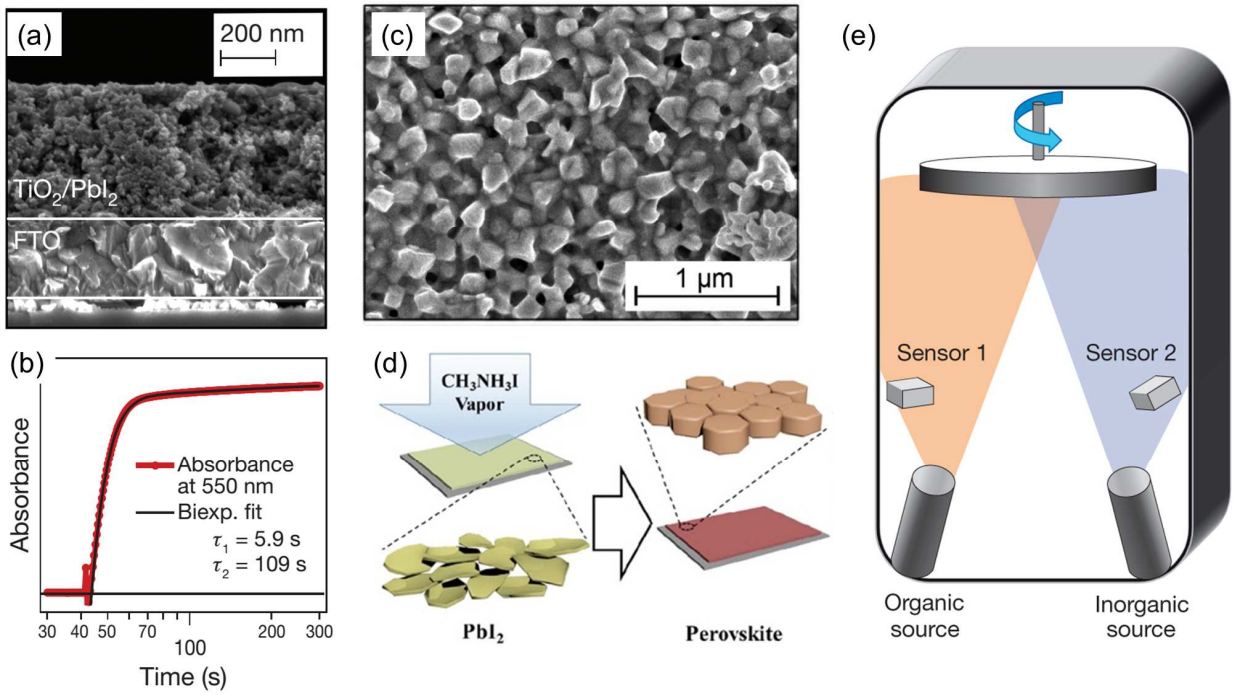

Figure 5: (a) Cross-sectional SEM of a mesoporous TiO_2 film infiltrated with PbI_2. (b) Change in absorbance at 550 nm of such a film monitored during the transformation from PbI_2 to $CH_3NH_3PbI_3$. (c) Top view of $CH_3NH_3PbI_3$ film obtained using the sequential deposition method. (d) An illustration of the vapour assisted transformation of PbI_2 to $CH_3NH_3PbI_3$ by exposure to CH_3NH_3I vapour. (e) Dual-source thermal evaporation system for depositing the perovskite absorbers; the organic source was methylammonium iodide and the inorganic source $PbCl_2$. (a) - (c) are reproduced from ref. 35 copyright 2013, Nature Publishing Group; (d) is reproduced from ref. [56] copyright 2013, American Chemical Society and (e) is reproduced from ref. [55] copyright 2013, Nature Publishing Group.

Apart from the widely utilised solution-based deposition processes, vapour deposition has also been employed to form perovskite solar cells. Snaith and coworkers[55] demonstrated efficient planar solar cells (15.4%) of $CH_3NH_3PbI_{3-x}Cl_x$ formed by dual source evaporation of $PbCl_2$ and CH_3NH_3I (Figure 5(e)). The evaporated film was sandwiched between a compact TiO_2 layer and a spuncoated Spiro-OMeTAD layer acting as electron and hole transporters respectively. The vapour-deposited films are extremely uniform, with crystalline features on the length scale of hundreds of nanometres. Another example of vapor deposition was demonstrated by Bolink and coworkers[62] who deposited thin films of $CH_3NH_3PbI_3$ from the dual source evaporation of PbI_2 and CH_3NH_3I. The authors employed organic electron and hole transport layers such as PCBM and PEDOT:PSS to form solar cells with 12.04% efficiency. Both the dual source evaporation examples described above required careful optimization to yield the desired perovskite layers and efficient solar cells. An interesting approach which employs both solution based deposition and vapor phase transformation has been reported by Chen et.al.[56] In the vapor-assisted solution process (VASP), PbI_2 was first deposited from solution on to a compact TiO_2 substrate. Subsequently, the films were exposed to a vapour of CH_3NH_3I at 150^{o}C in N_2 for 2h (Figure 5(d)). The slow rate of conversion resulted in $CH_3NH_3PbI_3$ films which exhibited micron sized grains with very low surface roughness of ~20 nm. Solar cells made from such films exhibited an efficiency of 12.1%.

In conjunction with these exciting device-centric advancements, fundamental studies into the photoexcited species and their photogeneration and recombination dynamics in perovskites also began in earnest. The next section traces these early studies to the latest findings of the fundamental photophysical mechanisms in this system.

4. Photophysical Mechanisms in $CH_3NH_3PbI_3$ Thin Films

The early photophysical studies in this class of organic-inorganic perovskites are mainly centered on the excitonic properties of layered perovskites such as the optical non-linearity around the excitonic resonances[63] and the exciton-exciton interactions[64]. Coherent transient spectroscopy such as four wave mixing has been used to investigate the exciton and bi-exciton dynamics[65] and temperature dependent TRPL spectroscopy for the exciton recombination dynamics[66] in these 2D perovskites. Depending on the exciton binding energy E_b, the fundamental excited species following photoexcitation could exist as bound electron-hole pairs or as free carriers. Hence, E_b have also been extensively investigated for $CH_3NH_3PbI_3$, the photovoltaic material of choice. **Table 1** shows the E_b, of selected 3-D perovskites with low-dimension perovskites included for comparison. These E_b are estimated using optical absorption[7] and magneto-absorption spectra[67, 68] as well as from temperature-dependent photoluminescence (PL)

intensities[45, 69]. The excitons in $CH_3NH_3PbI_3$ are expected to be of the more delocalized Wannier-type with exciton Bohr radius, r_B ~30 Å.[7, 70] Larger binding energies for $CH_3NH_3PbBr_3$ and the mixed halide $CH_3NH_3PbI_{3-x}Cl_x$ system indicates a more tightly bound nature of the excitons resulting from the halogen substitution. In contrast, for 2-D layered perovskites, the excitons are the Frenkel type and their large binding energies are ascribed to dielectric modulation between the organic and inorganic layers and the two dimensionality of the inorganic structure.[71] With decreasing dimensionality to 1-D and 0-D, the exciton binding energies increase in accordance to the quantum confinement effects.[70]

Table 1: Exciton binding energies E_b of the 3-D $CH_3NH_3PbI_3$ and $CH_3NH_3PbI_{3-x}Cl_x$ perovskites and selected low-dimension perovskites.

Compound	Dimensionality	E_b (meV)	Method
$CH_3NH_3PbI_3$	3D	30	optical absorption[7]
		37	magneto-absorption[67]
		45	temperature dependent PL[69]
		50	magneto-absorption[68]
		19±3	temperature dependent PL[45]
$CH_3NH_3PbBr_3$	3D	76	magneto-absorption[68]
		150	optical absorption[7]
$CH_3NH_3PbI_{3-x}Cl_x$	3D	98	temperature dependent PL[72]
$(C_9H_{19}NH_3)_2PbI_4$	2D	≥ 330	temperature dependent PL[69]
$(NH_2C(I)=NH_2)_3PbI_5$	1D	≥ 410	optical absorption[7]
$(CH_3NH_3)_4PbI_6.2H_2O$	0D	545	optical absorption[7]

Absorption of photons creates electron-hole pairs in the perovskite. Following carrier thermalization, these carriers could either continue to exist as free carriers or form excitons depending on the excitons binding energy. Presently, it is still unclear whether these species at room temperature exist as excitons or free charges – which gave rise to the 3-D perovskite's exceptional properties of long diffusion lengths. This uncertainty stems from the low exciton binding energies E_b ranging from 19 meV to 50 meV, which are comparable to the room temperature thermal energies of k_BT ~25 meV. Given the uncertainties and the assumptions involved with the estimation/extraction of the values for E_b based on the various methods employed (optical absorption[73, 74], magneto-absorption[68] and temperature dependent PL[75]), it is reasonable from **Table 1** that the E_b for $CH_3NH_3PbI_3$ is comparable to the thermal energies of k_BT ~ 25 meV at room temperature. As an illustration, even for an E_b ~19 meV, the faction of the excitons with energy greater than E_b at ~300K can be calculated from statistical physics to yield: ~57% of the photo-generated excitons dissociating spontaneously and ~43% remaining as excitons. It is an open question on how the co-existence of free carriers and excitons, whose dynamic populations could vary over their lifetimes, will affect the carrier dynamics in perovskite solar cells.

To the best of our knowledge, there have been no reported studies on the charge dynamics in 3D perovskites until the advent of the 9.7% perovskite solar cells in 2012[32]. Despite the rapid progress in organic-inorganic perovskite solar cells, the fundamental photophysical processes driving the high performance of these devices is still severely lacking. The bulk of the research efforts to date are predominantly focused on device development, with limited studies on charge carrier dynamics in the $CH_3NH_3PbI_3$ perovskite materials.[32, 33, 46, 76-78] Nevertheless, the efforts into applying ultrafast optical spectroscopy (UOS) techniques to investigate the structure-function relations in perovskite solar cells are on the rise. UOS techniques are powerful probes of the carrier dynamics and the charge transfer mechanisms in materials. A clear understanding of the charge generation and transport mechanisms in perovskites solar cells will provide valuable feedback to guide the materials design and device engineering. Here, we first examine the intrinsic charge dynamics in the bare perovskite thin films. The charge transfer processes in a typical perovskite solar cell will be examined in the next section.

Long Electron-Hole Diffusion Lengths and Hot Hole Cooling Dynamics: In tandem with the developments of increasing perovskite solar cell efficiencies, indications of ambipolar charge transport in perovskites become apparent when efficient perovskite-based devices in a broad range of device architectures are reported. The perovskite material functions well as an absorber in a configuration used by Kim *et. al.*[32] and Heo *et. al.*[34] that sandwiches the thin perovskite layer between a mesoporous TiO_2 photoanode and a HTM layer (Spiro-OMeTAD). Lee *et. al.*[33] demonstrated that the perovskite material can work effectively as both an absorber and an electron transporter by fabricating solar cells with an insulating Al_2O_3 scaffold instead of the TiO_2 photoanode. Surprisingly, Etgar *et. al.*[38] fabricated devices with appreciable performance in a configuration without the HTM layer – indicating that the perovskite material can work as an absorber and a hole transporter.

These reports provide us with a compelling case to devise quenching experiments utilizing femtosecond transient optical spectroscopy (*i.e.*, TAS and time-resolved PL (TRPL) spectroscopy) of $CH_3NH_3PbI_3$ heterojunctions with selective electron or hole extraction to decouple the electron and hole dynamics in this material.[46] Our findings revealed clear evidence of balanced and long-range electron-hole diffusion lengths of <u>*at least*</u> 100 nm in the solution processed $CH_3NH_3PbI_3$ (Figure 6). Concurrently, using the same PL quenching approach, H. J. Snaith and coworkers[77] also performed diffusion length measurements on $CH_3NH_3PbI_3$ and the mixed halide $CH_3NH_3PbI_{3-x}Cl_x$. Their findings of the electron-hole diffusion lengths in $CH_3NH_3PbI_3$ concur with ours. Amazingly, the mixed halide $CH_3NH_3PbI_{3-x}Cl_x$ possesses diffusion lengths one order longer (*i.e.*, >1 μm) than $CH_3NH_3PbI_3$, although no clear reason was identified for this difference. Nevertheless, these two works clearly show that the electron-hole diffusion

lengths in perovskites are much longer than those for most solution processed materials (typically ~10 nm). Most recently, G. Giorgi *et. al.*'s spin-polarized DFT calculations determined the effective masses of both the electron and hole in $CH_3NH_3PbI_3$ to be small, (*i.e.*, $m_e^* = 0.23\ m_0$ and $m_h^* = 0.29$), thus providing further validation of their long-range ambipolar charge transport property [46, 77].

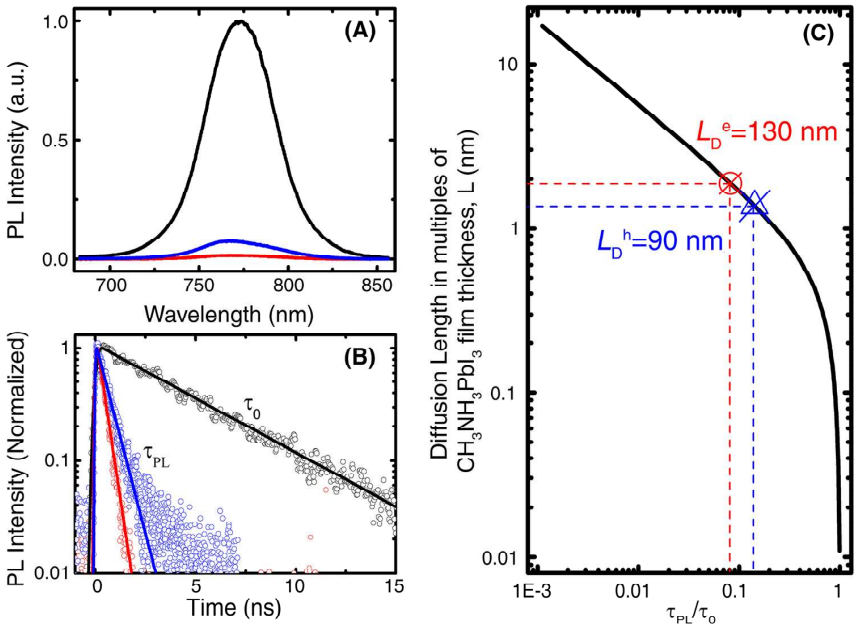

Figure 6: (A) Time-integrated PL spectra and (B) Time-resolved PL decay transients measured at 760 ± 10 nm for quartz/$CH_3NH_3PbI_3$(65 nm) (black), quartz/$CH_3NH_3PbI_3$ (65 nm)/PCBM (red), quartz/$CH_3NH_3PbI_3$(65 nm)/Spiro-OMeTAD (blue) films in vacuum after excitation at 600 nm (1 KHz, 150 fs, 1.3 μJ/cm^2). The solid lines in (B) are the single-exponential fits of the PL decay transients. a.u., arbitrary units. (C) A plot of exciton diffusion length versus PL lifetime quenching ratios. Diffusion length is scaled in multiples of $CH_3NH_3PbI_3$ layer thickness (L = 65 nm). Reproduced with permission from ref. 46, Copyright 2013, Science (AAAS).

In this same work, we also examined the early time relaxation dynamics in the $CH_3NH_3PbI_3$ system. It is important to note that the carrier dynamics in the perovskite system are strongly pump fluence dependent due to their large light absorption coefficients and the long charge diffusion lengths. Multi-particle Auger (third order) recombination processes becomes dominant for pump fluence >2.6 μJ/cm^2. In fact, we recently discovered that at pump fluence >12 μJ/cm^2, amplified spontaneous emission (ASE) prevails and even out-competes the Auger processes.[79] Therefore, careful control of the pump fluence in ultrafast optical spectroscopy of perovskites is absolutely essential for uncovering their intrinsic photophysical properties. Femtosecond TAS measurements with selective 400 nm and 600 nm pump excitation (fluence <1.3 μJ/cm^2) and WLC probe uncovered a slow 0.4 ps hot hole cooling process from a deeper valence band level (VB2) to the valence bandedge (VB1) – see Figure 7. With careful tailoring of the HTM's energy levels, one could efficiently extract these hot hole energies before they

cool down to VB1. Potentially, this could be utilized in perovskite solar cells to exceed the theoretical Shockley-Queisser limit.[80] Further investigations into this area should be conducted.

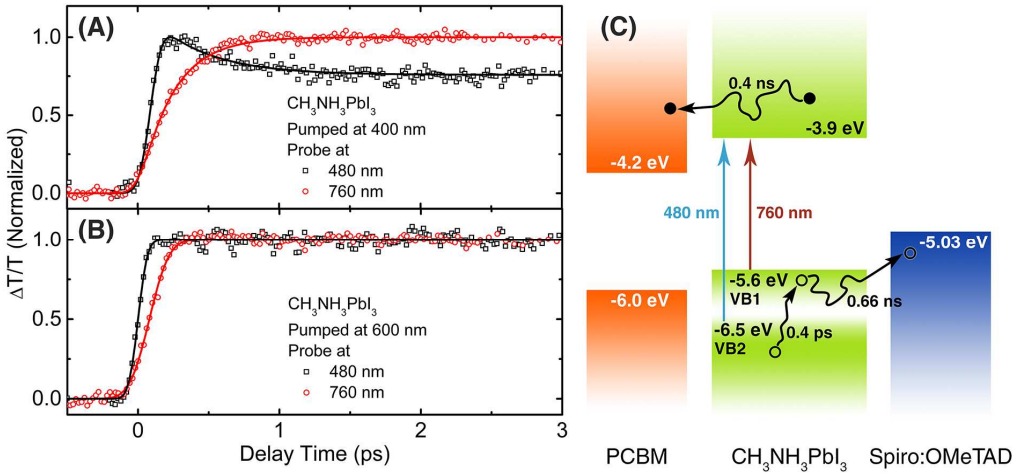

Figure 7: Normalized bleaching kinetics at 480 and 760 nm in a short time range show the intervalence band hot hole cooling for $CH_3NH_3PbI_3$ film (in vacuum) after excitation at (A) 400 nm (1 μJ/cm^2) and (B) 600 nm (1.3 μJ/cm^2). (C) A schematic illustrating the hot-hole cooling and charge recombination within $CH_3NH_3PbI_3$ and charge separation at the $CH_3NH_3PbI_3$/PCBM and $CH_3NH_3PbI_3$/Spiro-OMeTAD interfaces. The approximate positions of VB1 and VB2 were obtained from the TA measurements. Reproduced with permission from ref. 46, Copyright 2013, Science (AAAS).

Origins of the Long Electron-Hole Diffusion Lengths: The mechanism of the long electron-hole diffusion lengths in $CH_3NH_3PbI_{3-x}Cl_x$ and $CH_3NH_3PbI_3$ and their charge carrier mobilities were elucidated by L. M. Herz in collaboration with H. J. Snaith and coworkers[78] using transient THz spectroscopy. Their findings show that both the monomolecular (first order, *i.e.*, from germinate recombination of excitons and/or from trap- or impurity-assisted recombination) and bimolecular (second order) charge carrier recombination rates are extremely low, with the latter defying the Langevin limit by at least four orders of magnitude. However, the Auger (third order) recombination rates, were found to be high ~10^{-29} cm^{6}s^{-1} – comparable to those of strongly confined colloidal quantum dots.[81] Comparatively, the Auger recombination in highly-doped bulk Si wafers is ~2 orders smaller.[82] The lower bound values of the charge carrier mobilities for $CH_3NH_3PbI_{3-x}Cl_x$ and $CH_3NH_3PbI_3$ were determined to be 11.6 cm^{2}V^{-1}s^{-1} and ~8 cm^{2}V^{-1}s^{-1}, respectively, which are extremely high for the solution-processed perovskites. Comparatively, these values are >20 times larger than that of mesoporous TiO_2 and several orders larger than those of typical π-conjugated molecular semiconductors. The origins of the long electron-hole diffusion lengths stems from the exotic combination of low charge carrier recombination rates and high charge carrier mobilities in these perovskites.

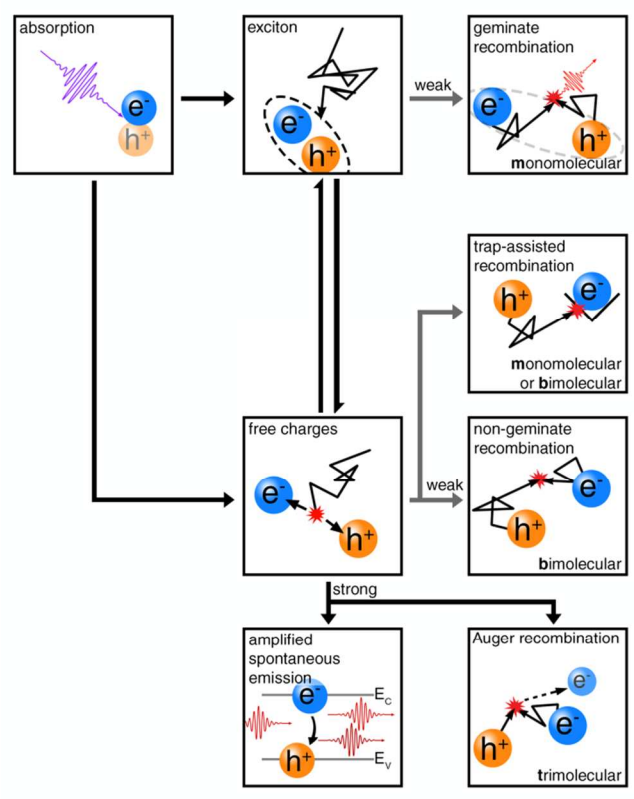

Figure 8: A schematic of the photophysical processes and loss mechanisms in perovskites following photoexcitation. Efficient paths (black lines) and suppressed paths (grey lines). Monomolecular recombination is charge carrier density independent, while bi-molecular and Auger recombination are charge carrier density dependent processes that would typically be present under strong photoexcitation. In fact, under even higher photoexcitation densities, amplified spontaneous emission (ASE) will out-compete Auger recombination. However, under solar light intensities (weak excitation), these latter processes will be strongly suppressed.

Summary of Photophysical Processes in Pristine Films: A generalized scheme of the dynamic interplay of the various photophysical processes and loss mechanisms in bare perovskite thin films following photoexcitation is shown in Figure 8. Absorption of photons results in the generation of electron-hole pairs that evolve towards the formation of highly delocalized Waniner excitons after thermalization. A faction of which would dissociate spontaneously back into free carriers. The excitons and free carriers coexist and their dynamic populations continue to vary over their lifetimes. Germinate recombination of the excitons, or the recombination involving an electron and a hole generated from the quenching of a single exciton is inefficient. Likewise, trap-assisted recombination, another monomolecular process, is also suppressed in these $CH_3NH_3PbX_3$ perovskites. At stronger light intensities, non-germinate recombination originating from the recombination of two free charges (*i.e.*, bi-molecular in nature) is extremely low – defying the traditional Langevin limit by at least four orders of magnitude. Auger recombination (involving a three particle process) on the other hand is dominant in $CH_3NH_3PbX_3$

perovskites and surprisingly, ASE even occurs at higher pump excitations – out-competing the Auger processes in $CH_3NH_3PbI_3$.[79] Eventually, in these bare perovskite films without HTM and in the absence of any charge extraction, the photoexcited species (excitons and free carriers) undergo radiative (luminescence) or non-radiative processes within the perovskite. It is also important to note that under solar light intensities (weak excitation), Auger recombination or ASE would be strongly suppressed. With the non-radiative pathways (germinate recombination, trap-assisted recombination and Auger recombination) weak or inactive under solar light intensities, it is therefore understandable that these perovskites make excellent photovoltaic materials.

5. Charge Transfer Mechanisms in Perovskite Solar Cells

As described previously, various configurations of perovskite solar cells have been explored. These include the configurations where perovskite has been interfaced with mesoporous TiO_2, mesoporous Al_2O_3 (MSSC) as well as other organic electron and hole transport layers. Ultrafast measurements have clearly indicated that $CH_3NH_3PbI_3$ and $CH_3NH_3PbI_{3-x}Cl_x$, both have long and balanced electron-hole transport lengths.[46, 77] It has also been clearly shown that injection into electron acceptors such as PCBM and hole transporters such as PEDOT:PSS and Spiro-OMeTAD is efficient.[46, 53, 59, 77] Thus, planar configurations of perovskite solar cells can be expected to function as thus: under photoexcitation, a mixture of weakly bound excitons and direct electron, hole generation occurs. Due to the crystalline nature of the perovskite as well as low trap densities, the recombination within the perovskites is limited. The long-lived nature of electrons and holes allows them to be collected by electron and hole acceptor layers, before making their way out of the solar cells as photocurrent. The high open circuit voltages noted in such planar configurations also point to a scenario where energetic costs associated with exciton splitting is not prevalent. Light intensity dependent measurements on a PEDOT:PSS/$CH_3NH_3PbI_{3-x}Cl_x$ / PCBM solar cell indicate that the main recombination mechanism is free carrier recombination.[59] The meso-superstructured solar cells[33, 36, 50, 51] which utilize an insulating mesoporous layer as a scaffold for the perovskite can be expected to work in a similar manner. Here the primary charge separation phase is probably the hole transporting layer (Spiro-OMeTAD) into which hole injection occurs efficiently. The good electron transport properties of the perovskite layer ensure that electrons are collected through the compact TiO_2 layer below the insulating mesoporous layer. Thus, a connected perovskite layer within the mesoporous layer is critical. The exact working principle behind solar cells fabricated by depositing perovskite on a mesoporous TiO_2 layer is still not clearly established. The pertinent questions when considering this architecture are: (a) Is there injection of electrons from the perovskite into mesoporous TiO_2; (b) Is the more efficient path for electron collection through the

mesoporous TiO_2 or within the perovskite itself? (c) Which pathway results in higher extraction efficiency in perovskite solar cell?

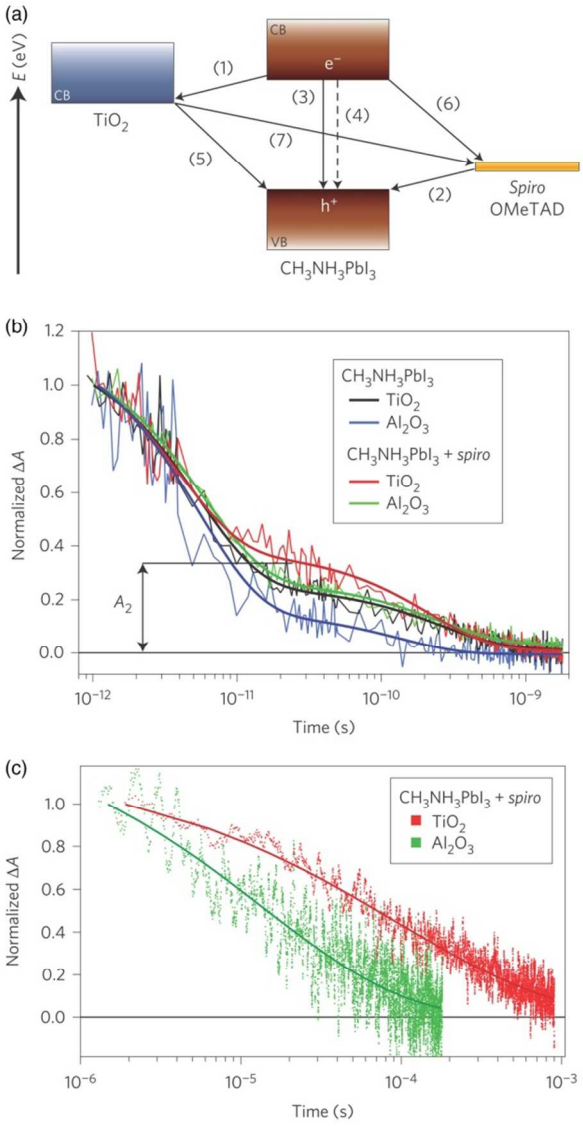

Figure 9: (a) Schematic diagram of energy levels and electron transfer processes in an HTM/perovskite/TiO_2 cell. (1): Electron Injection; (2): Hole injection; (3): Radiative exciton recombination; (4) Non-radiative exciton recombination; (5) Back electron transfer at the TiO_2 surface; (6) Back charge transfer at the HTM surface; (7) Charge recombination at the TiO_2/HTM interface. (b) Transient absorption signals were measured at a probe wavelength of 1.4 μm following femtosecond- laser pulsed excitation at 580 nm: $CH_3NH_3PbI_3$ on TiO_2 (black); $CH_3NH_3PbI_3$ on Al_2O_3 (blue); $CH_3NH_3PbI_3$ and spiro-OMeTAD on TiO_2 (red); $CH_3NH_3PbI_3$ and spiro-OMeTAD on Al_2O_3 (green). Thick solid lines represent bi-exponential fits of experimental points starting at t = 1 ps. A_2 represents the normalized absorbance change at 25 ps, used as a metric to compare the various samples. (c) Samples with HTM. Signals mainly reflect the decay of the h^+ (HTM) population. $CH_3NH_3PbI_3$ and spiro-OMeTAD on TiO_2 (red); $CH_3NH_3PbI_3$ and spiro-OMeTAD on Al_2O_3 (green). Thick lines represent stretched exponential fit of data. Reproduced with permission from ref. [83] , copyright 2014, Nature Publishing Group.

N. G. Park in collaboration with M. Grätzel and coworkers[32] published the earliest study on the dynamics of the charge separation processes in $CH_3NH_3PbI_3/TiO_2$ solar cells probed using femtosecond transient absorption spectroscopy (fs-TAS). However, clear evidence of efficient electron injection into TiO_2 could not be observed due to the overlapping signals from the stimulated emission from the perovskite. Although the question on whether perovskite can inject an electron into the mesoporous TiO_2 has more or less been answered by photoinduced absorption spectroscopy (PIA) from the evidence of a broad absorption feature in the region ~1.1 μm attributed to free electrons in the titania from $CH_3NH_3PbI_{3-x}Cl_x$ [33, 84], clear evidence of the efficient injection remain elusive. Most recently, J.-E. Moser in collaboration with M. Grätzel and coworkers unravelled the mechanism of the charge transfer processes in perovskite solar cells (Figure 9(a)) and presented clear evidence of not only efficient electron injection from the photoexcited $CH_3NH_3PbI_3$ into TiO_2, but also efficient hole injection from photoexcited $CH_3NH_3PbI_3$ into the HTM (spiro-OMeTAD) occurring simultaneously over comparable ultrafast timescales (≤ 3ps).[83] They had overcome the challenges of spectral overlap encountered in the earlier study[32] by probing in the infrared (1.4 μm) which allows direct observation of only the carrier's population decay within the perovskite itself (Figure 9(b)).

The second and third questions on whether electron collection is more efficient through the mesoporous TiO_2 or within the perovskite itself; and which pathway results in higher extraction efficiency in perovskite solar cells remain open. H. J. Snaith in collaboration with T. N. Murakami and T. Miyaska and coworkers[33], showed using transient photocurrent measurements that the charge collection in the insulating Al_2O_3-based devices is faster than the TiO_2-based devices – indicating the perovskite material itself is more efficient in transporting negative charge than the mesoporous TiO_2. However, recent findings by Marchioro *et. al.* using transient absorption spectroscopy showed that the amount of long-lived charges in the $TiO_2/CH_3NH_3PbI_3$/HTM samples is higher than that in the $Al_2O_3/CH_3NH_3PbI_3$/HTM samples (Figure 9(b)) – indicating a more efficient charge separation in the former. Furthermore, charge recombination with oxidized HTM species was also found to be slower on TiO_2 films compared to Al_2O_3 films (Figure 9(c)). The efficiency of charge extraction in a perovskite solar cell also depends on the ratio between charge recombination and charge separation rates. Nevertheless, Marchioro *et. al.'s* findings showed that it is advantages to use TiO_2 as the electron acceptor and transporter, together with HTM in perovskite solar cells – providing only partial answers to question 3.

Impedance spectroscopy measurements have also been applied to perovskite solar cells in a bid to understand the electrical processes occurring in them. Bisquert and coworkers analysed perovskite solar cells on TiO_2 and ZrO_2 and proposed that carrier accumulation occurs in the perovskite layers.[85] This

indicates that the working principle of the perovskite solar cells is different from that of a pure DSSC where instantaneous injection from the dye into the TiO_2 occurs and no charge accumulation is observable in the light absorber. Dualeh *et.al.* in their impedance spectroscopy analysis have argued that the observation of the mesoporous TiO_2's chemical capacitance in perovskite solar cells indicates that the electron transport is channeled through the mesoporous TiO_2.[86] The capacitance of TiO_2 in perovskite solar cells has also been observed by Abrusci *et. al* in their differential capacitance measurements when employing a C_{60}-self assembled monolayer on top of the TiO_2 surface.[84] Zhu and coworkers also point to a similar working mechanism in solid state DSCs and perovskite solar cells dominated by electron transport within the mesoporous TiO_2 layer itself, from intensity modulated photocurrent/photovoltage spectroscopy (IMPS/IMVS) measurements.[87] However Bisquert and coworkers have reported a similar impedance spectral shape in planar $CH_3NH_3PbI_{3-x}Cl_x$ and nanostructured $CH_3NH_3PbI_3$ solar cells. Since there is an absence of the TiO_2 mesoporous layer in one of the devices, they attribute the features in the impedance spectra to charge transport and recombination processes occurring within the perovskite layer solely. The authors have also noted that more complicated impedance spectra pattern can be observed in other cases which necessitate the development of a complete model.

The unclear view of the exact working principles of perovskite-mesoporous TiO_2 solar cells could stem from the variations in the solar cell structures studied and their ensuing interfacial charge transfer dynamics. The impact of the degree of coverage of the mesoporous TiO_2 by the perovskite is unclear. The presence or absence of a perovskite overlayer on the mesoporous TiO_2 will modulate the recombination at the perovskite/TiO_2/HTM interfaces. Additionally the distribution of the perovskite within the TiO_2 pores may also play a defining role in what mechanism of electron transport dominates. For example, charge transport time in $CH_3NH_3PbI_3$ formed from sequential deposition process was found to be 3 times longer than that obtained from the single precursor spincoating process.[36] From spectroscopic evidence, it is clear that charge injection from perovskite into mesoporous TiO_2 is possible[33, 83, 84]; however the exact ratio between electrons being transported through the mesoporous TiO_2 and that transported through the perovskite is unknown. Possibly, spectroscopic measurements in working solar cells at different applied voltages may unravel this question.

6. Future Directions and Open Questions in the Field

In the wake of the rapidly expanding field, several pressing open questions remain. They have been largely swept aside in the initial surge for high efficiencies. As the perovskite photovoltaic field matures, these gaps in our understanding need to be progressively tackled and filled:

Interfacial Charge Transfer Dynamics: For any given material system, factors such as device processing and the ensuing morphology and coverage can strongly affect the carrier dynamics and the device performance. Systematic studies into understanding the morphology effects arising from the single precursor vs sequential deposition solution-processed approach or thermal evaporation approach on the charge dynamics in the pristine and heterojunctions perovskite films are urgently needed. Given that the 100 nm e-h diffusion lengths estimated from the single step processed $CH_3NH_3PbI_3$ are *minimum values*[46], further work is urgently needed to carefully examine the e-h diffusion lengths in sequential deposited films and evaporated films to establish their upper limits. Over the next phase of development in this field, one can look forward to an explosion of systematic transient spectroscopy studies of various pristine/heterojunction configurations over the entire charge generation to charge extraction timescale, in particular: (i) the dynamic interplay and interactions between the excitons and the free charge population and their effects on the charge separation, recombination and transport; (ii) the interfacial charge dynamics and the mechanism of the charge injection at the perovskite/mesoporous TiO_2; perovskite/semiconductor nanostructure; and perovskite/graphene interfaces; and (iii) the exact role of higher lying states (if any) for charge separation. Time-resolved optical pump-terahertz probe spectroscopy would be extremely useful to monitor the early time excitons and free-carrier dynamics and populations in the pristine films and heterojunctions. These studies could be extended with transient microwave photoconductance measurements over longer time scales for correlation with device properties. Double excitation techniques like the pump-push probe spectroscopy can be used to study the higher lying electronic states and their roles in the charge transfer. Field modulation techniques like field assisted pump-probe spectroscopy could also lead to new insights on the interplay of the exciton dissociation and the free carrier dynamics on the charge transfer under device conditions. With the concerted efforts of various research groups, a complete picture and detailed model of the charge transfer processes of perovskite solar cells will be unravelled. Understanding the structure-function relations in perovskite solar cells through UOS holds the key to the development of optimal solar cells with efficiencies that could surpass the 20% target.

$CH_3NH_3PbI_3$ vs $CH_3NH_3PbI_{3-x}Cl_x$: Highly efficient solar cells have been prepared from $CH_3NH_3PbI_3$ and $CH_3NH_3PbI_{3-x}Cl_x$. The precursor solution of the latter compound consists of 3 parts of CH_3NH_3I for 1 part of $PbCl_2$. Although initial studies had termed the mixed composition as $CH_3NH_3PbI_2Cl$, the crystallographical and optical absorption properties are identical to that of $CH_3NH_3PbI_3$.[33] Stranks *et.al*. have shown,[77] the diffusion lengths measured in $CH_3NH_3PbI_{3-x}Cl_x$ are significantly longer than that in $CH_3NH_3PbI_3$, although the device performance of both compositions are comparable. In addition, while the charge carrier mobilities in both $CH_3NH_3PbI_{3-x}Cl_x$ and $CH_3NH_3PbI_3$ are similar, the bimolecular

recombination rates in the mixed halide system are approximately one order lower, suggesting that electronic structure modulation by Cl has a role in reducing the spatial overlap of the electron and holes.[78] Colella *et. al.* have also proposed that Cl within $CH_3NH_3PbI_3$ can act as a dopant, improving the transport properties.[88] XPS measurements have revealed that the final composition of the $CH_3NH_3PbI_{3-x}Cl_x$ contains significantly low amount of Cl (Cl/Cl+I=2.2%) within them.[59] XRD analysis of evaporated $CH_3NH_3PbI_{3-x}Cl_x$ films[55] also revealed impurity peaks of PbI_2, although the precursors were $PbCl_2$ and CH_3NH_3I. This points to the Cl source (either $PbCl_2$ or CH_3NH_3Cl) playing a role in the film formation. The development of a preferred orientation in $CH_3NH_3PbI_{3-x}Cl_x$ films[33] in contrast to $CH_3NH_3PbI_3$ films[35] again indicates that the Cl plays a role in film formation. Studies on $CH_3NH_3PbI_3$ and $CH_3NH_3PbI_{3-x}Cl_x$ films with similar film properties (morphological and crystallographical) are required, to reveal the electronic role of Cl within the perovskite.

Hole Transporting Layers: The hole transporting material of choice for perovskite solar cells is spiro-oMeTAD, which has been well studied due to its popularity in solid-state DSCs. However, the high commercial prices of spiro-oMeTAD (due to synthesis complexity) as well as its tendency to be uncontrollably doped by O_2, necessitate the development of other alternatives. The wide variety of hole transporting organic layers originally developed for organic thin film transistors as well as light emitting devices could possibly be applied in conjuction with the perovskite system. An early study on alternatives to Spiro-oMeTAD for perovskite solar cells, had indicated that thiophene based systems may not be suitable.[34] Arylamine based hole transporters such as poly-triarylamine,[34] N,N-di-p-methoxyphenylamine-substituted pyrene derivatives[89] and swivel cruciform thiophene-based molecules[90] have shown performances between 11-12%. An interesting development[91] has been the utilisation of inorganic CuI hole transport layer with $CH_3NH_3PbI_3$. Although they performed worse than spiro-oMeTAD solar cells due to high recombination, the work does indicate the possibility of applying other inorganic hole transporters such as CuSCN to the perovskite system. An equally intriguing avenue is the application of nanocarbon (eg. Graphite, carbon nanotubes, graphene-polymer composites) based hole transporters. As has been pointed out by Johansson and coworkers, the efficiencies can be primarily determined by recombination at the perovskite-HTM interface.[76] The low thicknesses of HTM layers (~100 nm) in well optimised solar cells as well as the utilisation of dopants, point to very low losses within the HTM itself, indicating the crucial nature of the perovskite-HTM interaction.

Newer Perovskite Compositions: Much of the high efficiency solar cells have focussed on $CH_3NH_3PbI_3$ as the light absorber. Although this composition currently yields the most efficient solar cells, newer perovskite compositions which have tuneable bandgaps would be of interest to tandem solar cell

configurations or in power applications that require high voltages. Seok and coworkers have elegantly shown how partial substitution of I with Br can yield colourful solar cells with varying photocurrent onset. A benefit of the partial substitution also seems to be improved stability.[37] Similarly, Hodes and Cohen have demonstrated $CH_3NH_3PbBr_{3-x}Cl_x$ solar cells with open circuit voltages as high as 1.5V. [92] Another key effort required is the reduction of bandgap of the perovskite solar cells for increased spectral response and therefore improved efficiencies. $CH_3NH_3PbI_3$ based solar cells do not efficiently harvest photons close to its optical absorption onset (600-780 nm), resulting in photocurrents not approaching the theoretical maximum. The development of formamidinium ($HC(NH_2)_2^+$) lead perovskites[93-96] with a lower bandgap (1.48 eV) that allows for high photocurrents is thus a promising development. These high photocurrents allowed Eperon et. al to demonstrate planar heterojunction solar cells with power conversion efficiencies of upto 14.2%. [93] The most pressing demand for newer photoactive perovskites is driven by the need to replace Pb. Hodes has estimated that a production capacity of 1000 GW per year from $CH_3NH_3PbI_3$ solar cells requires less than 10,000 tons of lead – much lower than the 4 million tons per year of lead used for lead-acid batteries currently.[97] Thus, although the total amount of lead that is required is low, the risk of leaching Pb into the environment needs to be managed. Sn^{2+} may serve as a replacement to Pb^{2+}, but its tendency to be easily oxidised is drawback.[98] Computational predictions play a critical role in Pb replacement efforts, due to the large variety of halide perovskites possible.

Towards Printability and Scalability: The rapid growth in the efficiencies of perovskite solar cells within a short time period has been catalogued previously. [97, 99] A target of 20% PCE value has also been identified as attainable in the perovskite solar cells. However, as important as the pursuit of efficiency is the pursuit of development activities aimed at depositing the perovskite materials through scalable manufacturing techniques such as screen printing. Carnie *et.al* have demonstrated that Al_2O_3 nanoparticles can be mixed in directly with perovskite solution and spuncoated to form a composite photoactive layer. [51] Further development of similar process recipes could yield compositions that could be screen printed, blade coated or applied through slot die coating. A fully printable perovskite solar cells albeit with an unconventional device configuration has been demonstrated by Han and coworkers.[100] The device architecture consisted of a screen printed TiO_2 layer, ZrO_2 layer and a carbon black/ graphite composite layer onto which $CH_3NH_3PbI_3$ was dropcasted. Such devices displayed an efficiency of 6.64%. A critical barrier in the implementation of a printable perovskite solar cell is the deposition of the electron selective compact layer (typically TiO_2 formed by spray pyrolysis at high temperature). Planar perovskite solar cells employing organic electron and hole transport layers do not suffer from this limitation, but still display lower efficiencies than mesoporous layer based solar cells. [45, 53, 58, 59, 62] Approaches to avoid the high temperature process during the formation of the compact layer includes the utilization of

electrodeposited ZnO[41] or a spuncoated ZnO nanoparticle layer[57]. A similar nanoparticle based approach has been demonstrated by the utilization of a spuncoated graphene flake-TiO_2 nanoparticle layer as the compact layer yielding efficiencies of 15.6%. [101] Very recently, a new low temperature compact layer TiO_2 deposition recipe has yielded impressive efficiencies of up to 15.9% for a solar cell fabricated at temperatures less than 150°C.[102]

Table II: Compilation of high efficiency perovskite solar cells reported thus far (1st Feb 2014)

Report	Device structure	Device parameters	Efficiency	Active area
Sub-150 °C processed meso-superstructured perovskite solar cells with enhanced efficiency *Energy & Environmental Science* **2014**, *7,* 1142-1147.	FTO/TiO_2/mesoporous Al_2O_3/$CH_3NH_3PbI_{3-x}Cl_x$/Spiro-OMeTAD/Ag	J_{sc} = 21.5 mA/cm^2 V_{oc} = 1.02 V FF = 0.71	15.9%	0.0625 cm^2
Perovskite solar cells with a planar heterojunction structure prepared using room-temperature solution processing techniques. *Nat Photonics* **2014**, *8,*133-138	ITO/ZnO/$CH_3NH_3PbI_3$/Spiro-OMeTAD/Ag	J_{sc} = 20.4 mA/cm^2 V_{oc} = 1.03 V FF = 0.749	15.7%	0.07065 cm^2
Low-Temperature Processed Electron Collection Layers of Graphene/TiO2 Nanocomposites in Thin Film Perovskite Solar Cells *Nano Letters* **2014**, *14*, 724-730	FTO/Graphene-TiO_2/mesoporous-Al_2O_3/$CH_3NH_3PbI_{3-x}Cl_x$/Spiro-OMeTAD/Au	J_{sc} = 21.9 mA/cm^2 V_{oc} = 1.04 V FF = 0.73	15.6%	0.0625 cm^2
Efficient planar heterojunction perovskite solar cells by vapour deposition, *Nature* **2013**, *501*, 395-398.	FTO/TiO_2/$CH_3NH_3PbI_{3-x}Cl_x$/Spiro-OMeTAD/Ag	J_{sc} = 21.5 mA/cm^2 V_{oc} = 1.07 V FF = 0.67	15.4%	0.076 cm^2
Sequential deposition as a route to high-performance perovskite-sensitized solar cells, *Nature* **2013**, *499*, 316-319.	FTO/TiO_2/ mesoporousTiO_2/$CH_3NH_3PbI_3$ /Spiro-OMeTAD/Au	J_{sc} = 20 mA/cm^2 V_{oc} = 0.993 V FF = 0.73 J_{sc} = 21.3 mA/cm^2 V_{oc} = 1.0 V FF = 0.66	15.0% 14.1% (certified)	0.285 cm^2 0.209 cm^2

Much of the high efficiency reports on perovskite solar cells have been demonstrated on cell areas much less than 1 cm^2 (Table II). Malinkiewicz *et. al.* who reported an efficiency of 12.04% (cell area = 0.09cm^2) fabricated a ~1cm^2 solar cell using the same process which yielded an efficiency of 8.27%.[62] The primary difference in the photovoltaic parameters was the FF which reduced from 0.67 to 0.52 when going to the larger area solar cells. The reason for the reduction in the FF is unclear, but could arise from series resistance in the electrode itself. The first perovskite based modules have also been reported (up to 16.8 cm^2 module area) by Matteocci *et. al.* who employed both P3HT and Spiro-OMeTAD as hole transporters yielding efficiencies of 5.1%. [103] Such large scale demonstrations of perovskite solar cells are necessary for perovskite solar cells to develop into a technology for widespread deployment.

Stability studies: The 3-D methylammonium trihalogenoplumbates (II) crystals (*i.e.*, $CH_3NH_3PbCl_3$ $CH_3NH_3PbBr_3$ and $CH_3NH_3PbI_3$) are known to undergo 1st order phase transitions.[104, 105] In particular, $CH_3NH_3PbI_3$ undergoes a tetragonal I to cubic phase transition at ~327K (or ~54 ^{O}C), which is close to the device operating temperatures under direct sunlight. This cubic-tetragonal transition results in the methylammonium ions exhibiting a disordered character while the PbX_6 octahedron exhibiting a displacive character.[105, 106] Systematic studies on such effects on the carrier dynamics and on the device properties under operation are warranted. Since the phase transitions involve a volume change, it is pertinent to investigate whether infiltrating the perovskite within mesoporous layers, can improve temperature stability. Reports on long term device performance tests are few, with 500h stabilities under constant illumination being reported by Grätzel and coworkers.[35] Snaith and coworkers have reported performance data for 1000h in MSSCs and have pointed towards UV induced changes in TiO_2 based solar cells due to desorption of surface-adsorbed oxygen.[107] Systematic studies on the degradation mechanisms (including the hole transport layers) are required to manage the lifetimes of these solar cells. Newer perovskite compositions which do not undergo phase transitions at device operational temperatures should be pursued as well.

In summary, the field of perovskite solar cells has rapidly grown to become the most efficient solution processed photovoltaics, leapfrogging other 3rd generation photovoltaic technologies. As this field matures, rapid improvements in the power conversion efficiencies will become harder to come by. Thus, a deeper understanding of the fundamental working mechanisms become increasingly important- especially if efficiencies exceeding 20% need to be achieved. Concurrently, technological developments in the area of scalable manufacturing techniques, toxicity and stability need to be effectively addressed.

Acknowledgements

We would like to acknowledge Subodh Mhaisalkar and Pablo P. Boix for technical discussions and Tom Baikie and Swee Sien Lim for the figures. T.C.S. acknowledges the financial support from NTU start-up grant M4080514, SPMS collaborative Research Award M4080536, Ministry of Education AcRF Tier 2 grant MOE2013-T2-1-081. N.M. acknowledges the financial support from NTU start-up grant M4081293 and from Singapore National Research Foundation (NRF) through the Competitive Research Program (NRF-CRP4-2008-03). T.C.S. and N.M. also gratefully acknowledge the Singapore NRF for the funding through the Singapore-Berkeley Research Initiative for Sustainable Energy (SinBeRISE) CREATE Programme.

References

1. J. Nelson, *The Physics of Solar Cells*, Imperial College Press, 2003.
2. X. Wang, J. Byrne, L. Kurdgelashvili and A. Barnett, *Wiley Interdisciplinary Reviews: Energy and Environment*, 2012, 1, 132-151.
3. D. B. Mitzi, in *Progress in Inorganic Chemistry*, John Wiley & Sons, Inc., 2007, DOI: 10.1002/9780470166499.ch1, pp. 1-121.
4. T. Ishihara, World Scientific, Singapore ; River Edge, NJ, 1995, ch. Optical Properties of Pb-based inorganic-organic perovskites, pp. xix, 414 p.
5. K. A. Müller and T. W. Kool, *Properties of perovskites and other oxides*, World Scientific, Singapore ; Hackensack, NJ, 2010.
6. T. Ishihara, J. Takahashi and T. Goto, *Solid State Commun*, 1989, 69, 933-936.
7. I. B. Koutselas, L. Ducasse and G. C. Papavassiliou, *J Phys-Condens Mat*, 1996, 8, 1217-1227.
8. C. R. Kagan, D. B. Mitzi and C. D. Dimitrakopoulos, *Science*, 1999, 286, 945-947.
9. D. B. Mitzi, K. Chondroudis and C. R. Kagan, *Ibm J Res Dev*, 2001, 45, 29-45.
10. X. Hong, T. Ishihara and A. V. Nurmikko, *Solid State Commun*, 1992, 84, 657-661.
11. M. Era, S. Morimoto, T. Tsutsui and S. Saito, *Appl Phys Lett*, 1994, 65, 676-678.
12. C. Q. Xu, T. Kondo, H. Sakakura, K. Kumata, Y. Takahashi and R. Ito, *Solid State Commun*, 1991, 79, 245-248.
13. T. Kondo, S. Iwamoto, S. Hayase, K. Tanaka, J. Ishi, M. Mizuno, K. Ema and R. Ito, *Solid State Commun*, 1998, 105, 503-506.
14. A. Brehier, R. Parashkov, J. S. Lauret and E. Deleporte, *Appl Phys Lett*, 2006, 89.
15. J. Wenus, R. Parashkov, S. Ceccarelli, A. Brehier, J. S. Lauret, M. S. Skolnick, E. Deleporte and D. G. Lidzey, *Phys Rev B*, 2006, 74.
16. G. Lanty, S. Zhang, J. S. Lauret, E. Deleporte, P. Audebert, S. Bouchoule, X. Lafosse, J. Zuniga-Perez, F. Semond, D. Lagarde, F. Medard and J. Leymarie, *Phys Rev B*, 2011, 84.
17. Z. Han, H. S. Nguyen, F. Boitier, Y. Wei, K. Abdel-Baki, J. S. Lauret, J. Bloch, S. Bouchoule and E. Deleporte, *Opt Lett*, 2012, 37, 5061-5063.
18. Y. Wei, J. S. Lauret, L. Galmiche, P. Audebert and E. Deleporte, *Opt Express*, 2012, 20, 10399-10405.
19. G. C. Papavassiliou, *Progress in Solid State Chemistry*, 1997, 25, 125-270.
20. S. M. Wang, D. B. Mitzi, C. A. Feild and A. Guloy, *Journal of the American Chemical Society*, 1995, 117, 5297-5302.
21. Y. Kawamura, H. Mashiyama and K. Hasebe, *J Phys Soc Jpn*, 2002, 71, 1694-1697.
22. B. R. Vincent, K. N. Robertson, T. S. Cameron and O. Knop, *Canadian Journal of Chemistry*, 1987, 65, 1042-1046.
23. T. Umebayashi, K. Asai, T. Kondo and A. Nakao, *Phys Rev B*, 2003, 67.
24. Y. H. Chang, C. H. Park and K. Matsuishi, *J Korean Phys Soc*, 2004, 44, 889-893.
25. E. Mosconi, A. Amat, M. K. Nazeeruddin, M. Gratzel and F. De Angelis, *J Phys Chem C*, 2013, 117, 13902-13913.
26. T. Baikie, Y. N. Fang, J. M. Kadro, M. Schreyer, F. X. Wei, S. G. Mhaisalkar, M. Graetzel and T. J. White, *J Mater Chem A*, 2013, 1, 5628-5641.
27. Y. Wang, T. Gould, J. F. Dobson, H. Zhang, H. Yang, X. Yao and H. Zhao, *Phys. Chem. Chem. Phys.*, 2014, 16, 1424-1429.
28. J. Even, L. Pedesseau, J. M. Jancu and C. Katan, *Journal of Physical Chemistry Letters*, 2013, 4, 2999-3005.
29. B. O'Regan and M. Grätzel, *Nature*, 1991, 353, 737-740.

30. A. Kojima, K. Teshima, Y. Shirai and T. Miyasaka, *Journal of the American Chemical Society*, 2009, 131, 6050-6051.
31. J. H. Im, C. R. Lee, J. W. Lee, S. W. Park and N. G. Park, *Nanoscale*, 2011, 3, 4088-4093.
32. H. S. Kim, C. R. Lee, J. H. Im, K. B. Lee, T. Moehl, A. Marchioro, S. J. Moon, R. Humphry-Baker, J. H. Yum, J. E. Moser, M. Gratzel and N. G. Park, *Sci Rep-Uk*, 2012, 2.
33. M. M. Lee, J. Teuscher, T. Miyasaka, T. N. Murakami and H. J. Snaith, *Science*, 2012, 338, 643-647.
34. J. H. Heo, S. H. Im, J. H. Noh, T. N. Mandal, C. S. Lim, J. A. Chang, Y. H. Lee, H. J. Kim, A. Sarkar, M. K. Nazeeruddin, M. Gratzel and S. I. Seok, *Nat Photonics*, 2013, 7, 487-492.
35. J. Burschka, N. Pellet, S. J. Moon, R. Humphry-Baker, P. Gao, M. K. Nazeeruddin and M. Gratzel, *Nature*, 2013, 499, 316-319.
36. D. Bi, S.-J. Moon, L. Haggman, G. Boschloo, L. Yang, E. M. J. Johansson, M. K. Nazeeruddin, M. Gratzel and A. Hagfeldt, *Rsc Adv*, 2013, 3, 18762-18766.
37. J. H. Noh, S. H. Im, J. H. Heo, T. N. Mandal and S. I. Seok, *Nano Letters*, 2013, 13, 1764-1769.
38. L. Etgar, P. Gao, Z. S. Xue, Q. Peng, A. K. Chandiran, B. Liu, M. K. Nazeeruddin and M. Gratzel, *Journal of the American Chemical Society*, 2012, 134, 17396-17399.
39. H.-S. Kim, J.-W. Lee, N. Yantara, P. P. Boix, S. A. Kulkarni, S. Mhaisalkar, M. Grätzel and N.-G. Park, *Nano Letters*, 2013, 13, 2412-2417.
40. S. Dharani, H. K. Mulmudi, N. Yantara, P. T. Thu Trang, N. G. Park, M. Graetzel, S. Mhaisalkar, N. Mathews and P. P. Boix, *Nanoscale*, 2014, 6, 1675-1679.
41. M. H. Kumar, N. Yantara, S. Dharani, M. Graetzel, S. Mhaisalkar, P. P. Boix and N. Mathews, *Chem Commun*, 2013, 49, 11089-11091.
42. D. Bi, G. Boschloo, S. Schwarzmuller, L. Yang, E. M. J. Johansson and A. Hagfeldt, *Nanoscale*, 2013, 5, 11686-11691.
43. J. Burschka, A. Dualeh, F. Kessler, E. Baranoff, N. L. Cevey-Ha, C. Yi, M. K. Nazeeruddin and M. Grätzel, *Journal of the American Chemical Society*, 2011, 133, 18042-18045.
44. A. Yella, H.-W. Lee, H. N. Tsao, C. Yi, A. K. Chandiran, M. K. Nazeeruddin, E. W.-G. Diau, C.-Y. Yeh, S. M. Zakeeruddin and M. Grätzel, *Science*, 2011, 334, 629-634.
45. S. Sun, T. Salim, N. Mathews, M. Duchamp, C. Boothroyd, G. Xing, T. C. Sum and Y. M. Lam, *Energ Environ Sci*, 2014, 7, 399-407.
46. G. C. Xing, N. Mathews, S. Y. Sun, S. S. Lim, Y. M. Lam, M. Gratzel, S. Mhaisalkar and T. C. Sum, *Science*, 2013, 342, 344-347.
47. J. J. Choi, X. Yang, Z. M. Norman, S. J. L. Billinge and J. S. Owen, *Nano Letters*, 2013, DOI: 10.1021/nl403514x.
48. E. Enache-Pommer, B. Liu and E. S. Aydil, *Phys. Chem. Chem. Phys.*, 2009, 11, 9648-9652.
49. W. A. Laban and L. Etgar, *Energ Environ Sci*, 2013, 6, 3249-3253.
50. J. M. Ball, M. M. Lee, A. Hey and H. J. Snaith, *Energy & Environmental Science*, 2013, 6, 1739-1743.
51. M. J. Carnie, C. Charbonneau, M. L. Davies, J. Troughton, T. M. Watson, K. Wojciechowski, H. Snaith and D. A. Worsley, *Chem Commun*, 2013, 49, 7893-7895.
52. K. Wojciechowski, M. Saliba, T. Leijtens, A. Abate and H. J. Snaith, *Energ Environ Sci*, 2014, 7, 1142-1147.
53. P. Docampo, J. M. Ball, M. Darwich, G. E. Eperon and H. J. Snaith, *Nat Commun*, 2013, 4.
54. G. E. Eperon, V. M. Burlakov, P. Docampo, A. Goriely and H. J. Snaith, *Adv Funct Mater*, 2014, 24, 151-157.
55. M. Liu, M. B. Johnston and H. J. Snaith, *Nature*, 2013, 501, 395-398.
56. Q. Chen, H. Zhou, Z. Hong, S. Luo, H.-S. Duan, H.-H. Wang, Y. Liu, G. Li and Y. Yang, *Journal of the American Chemical Society*, 2013, 136, 622-625.
57. D. Liu and T. L. Kelly, *Nat Photonics*, 2013, DOI:10.1038/nphoton.2013.342.

58. J.-Y. Jeng, Y.-F. Chiang, M.-H. Lee, S.-R. Peng, T.-F. Guo, P. Chen and T.-C. Wen, *Adv Mater*, 2013, 25, 3727-3732.
59. J. You, Z. Hong, Y. Yang, Q. Chen, M. Cai, T.-B. Song, C.-C. Chen, S. Lu, Y. Liu and H. Zhou, *ACS Nano*, 2014, DOI: 10.1021/nn406020d, DOI:10.1021/nn406020d.
60. I. K. Ding, N. Tétreault, J. Brillet, B. E. Hardin, E. H. Smith, S. J. Rosenthal, F. Sauvage, M. Grätzel and M. D. McGehee, *Adv Funct Mater*, 2009, 19, 2431-2436.
61. K. Liang, D. B. Mitzi and M. T. Prikas, *Chem Mater*, 1998, 10, 403-411.
62. O. Malinkiewicz, A. Yella, Y. H. Lee, G. M. Espallargas, M. Graetzel, M. K. Nazeeruddin and H. J. Bolink, *Nat Photonics*, 2014, 8, 128-132.
63. R. Ito, S. Hayase, T. Kondo, S. Iwamoto, K. Ema, H. Kunugita, M. Mizuno and J. Ishi, *Journal of Nonlinear Optical Physics & Materials*, 1998, 07, 153-159.
64. M. Shimizu and J.-i. Fujisawa, *J Lumin*, 2004, 108, 189-194.
65. J. Ishi, H. Kunugita, K. Ema, T. Ban and T. Kondo, *Phys Rev B*, 2001, 63, 073303.
66. N. Kitazawa, M. Aono and Y. Watanabe, *Mater Chem Phys*, 2012, 134, 875-880.
67. M. Hirasawa, T. Ishihara, T. Goto, K. Uchida and N. Miura, *Physica B*, 1994, 201, 427-430.
68. K. Tanaka, T. Takahashi, T. Ban, T. Kondo, K. Uchida and N. Miura, *Solid State Commun*, 2003, 127, 619-623.
69. T. Ishihara, *J Lumin*, 1994, 60-1, 269-274.
70. M. Hirasawa, T. Ishihara and T. Goto, *J Phys Soc Jpn*, 1994, 63, 3870-3879.
71. X. Hong, T. Ishihara and A. V. Nurmikko, *Phys Rev B*, 1992, 45, 6961-6964.
72. W. Zhang, M. Saliba, S. D. Stranks, Y. Sun, X. Shi, U. Wiesner and H. J. Snaith, *Nano Letters*, 2013, 13, 4505-4510.
73. J. F. Muth, J. H. Lee, I. K. Shmagin, R. M. Kolbas, H. C. Casey, B. P. Keller, U. K. Mishra and S. P. DenBaars, *Appl Phys Lett*, 1997, 71, 2572-2574.
74. S. J. Zhang, P. Audebert, Y. Wei, A. Al Choueiry, G. Lanty, A. Brehier, L. Galmiche, G. Clavier, C. Boissiere, J. S. Lauret and E. Deleporte, *Materials*, 2010, 3, 3385-3406.
75. Z. Chen, C. L. Yu, K. Shum, J. J. Wang, W. Pfenninger, N. Vockic, J. Midgley and J. T. Kenney, *J Lumin*, 2012, 132, 345-349.
76. D. Bi, L. Yang, G. Boschloo, A. Hagfeldt and E. M. J. Johansson, *The Journal of Physical Chemistry Letters*, 2013, 4, 1532-1536.
77. S. D. Stranks, G. E. Eperon, G. Grancini, C. Menelaou, M. J. P. Alcocer, T. Leijtens, L. M. Herz, A. Petrozza and H. J. Snaith, *Science*, 2013, 342, 341-344.
78. C. Wehrenfennig, G. E. Eperon, M. B. Johnston, H. J. Snaith and L. M. Herz, *Advanced Materials*, 2013, DOI: 10.1002/adma.201305172, DOI: 10.1002/adma.201305172.
79. G. Xing, N. Mathews, S. S. Lim, N. Yantara, X. Liu, D. Sabba, M. Grätzel, S. Mhaisalkar and T. C. Sum, *Nat Mater*, 2014, 13, 476-480.
80. C. A. Nelson, N. R. Monahan and X. Y. Zhu, *Energ Environ Sci*, 2013, 6, 3508-3519.
81. V. I. Klimov, A. A. Mikhailovsky, D. W. McBranch, C. A. Leatherdale and M. G. Bawendi, *Science*, 2000, 287, 1011-1013.
82. J. Dziewior and W. Schmid, *Appl Phys Lett*, 1977, 31, 346-348.
83. A. Marchioro, J. Teuscher, D. Friedrich, M. Kunst, R. van de Krol, T. Moehl, M. Gratzel and J.-E. Moser, *Nat Photonics*, 2014, DOI:10.1038/nphoton.2013.374.
84. A. Abrusci, S. D. Stranks, P. Docampo, H.-L. Yip, A. K. Y. Jen and H. J. Snaith, *Nano Letters*, 2013, 13, 3124-3128.
85. H. S. Kim, I. Mora-Sero, V. Gonzalez-Pedro, F. Fabregat-Santiago, E. J. Juarez-Perez, N. G. Park and J. Bisquert, *Nat Commun*, 2013, 4.
86. A. Dualeh, T. Moehl, N. Tétreault, J. Teuscher, P. Gao, M. K. Nazeeruddin and M. Grätzel, *ACS Nano*, 2013, 8, 362-373.

87. Y. Zhao, A. M. Nardes and K. Zhu, *The Journal of Physical Chemistry Letters*, 2014, DOI: 10.1021/jz500003v, 490-494.
88. S. Colella, E. Mosconi, P. Fedeli, A. Listorti, F. Gazza, F. Orlandi, P. Ferro, T. Besagni, A. Rizzo, G. Calestani, G. Gigli, F. De Angelis and R. Mosca, *Chem Mater*, 2013, 25, 4613-4618.
89. N. J. Jeon, J. Lee, J. H. Noh, M. K. Nazeeruddin, M. Grätzel and S. I. Seok, *Journal of the American Chemical Society*, 2013, 135, 19087-19090.
90. K. Thirumal, K. Fu, P. P. Boix, H. Li, T. M. Koh, W. L. Leong, S. Powar, A. C. Grimsdale, M. Gratzel, N. Mathews and S. G. Mhaisalkar, *J Mater Chem A*, 2014, DOI: 10.1039/c4ta00486h, DOI: 10.1039/C1034TA00486H.
91. J. A. Christians, R. C. M. Fung and P. V. Kamat, *Journal of the American Chemical Society*, 2013, 136, 758-764.
92. E. Edri, S. Kirmayer, M. Kulbak, G. Hodes and D. Cahen, *The Journal of Physical Chemistry Letters*, 2014, 5, 429-433.
93. G. E. Eperon, S. D. Stranks, C. Menelaou, M. B. Johnston, L. M. Herz and H. J. Snaith, *Energ Environ Sci*, 2014, 7, 982-988.
94. N. Pellet, P. Gao, G. Gregori, T.-Y. Yang, M. K. Nazeeruddin, J. Maier and M. Grätzel, *Angewandte Chemie International Edition*, 2014, DOI: 10.1002/anie.201309361, DOI: 10.1002/anie.201309361.
95. T. M. Koh, K. Fu, Y. Fang, S. Chen, T. C. Sum, N. Mathews, S. G. Mhaisalkar, P. P. Boix and T. Baikie, *The Journal of Physical Chemistry C*, 2013, DOI: 10.1021/jp411112k, DOI: 10.1021/jp411112k.
96. S. Pang, H. Hu, J. Zhang, S. Lv, Y. Yu, F. Wei, T. Qin, H. Xu, Z. Liu and G. Cui, *Chem Mater*, 2014, 26, 1485-1491.
97. G. Hodes, *Science*, 2013, 342, 317-318.
98. C. C. Stoumpos, C. D. Malliakas and M. G. Kanatzidis, *Inorg Chem*, 2013, 52, 9019-9038.
99. N. G. Park, *Journal of Physical Chemistry Letters*, 2013, 4, 2423-2429.
100. Z. Ku, Y. Rong, M. Xu, T. Liu and H. Han, *Sci Rep-Uk*, 2013, 3, 3132.
101. J. T.-W. Wang, J. M. Ball, E. M. Barea, A. Abate, J. A. Alexander-Webber, J. Huang, M. Saliba, I. Mora-Sero, J. Bisquert, H. J. Snaith and R. J. Nicholas, *Nano Letters*, 2013, DOI: 10.1021/nl403997a.
102. K. Wojciechowski, M. Saliba, T. Leijtens, A. Abate and H. Snaith, *Energ Environ Sci*, 2013, DOI: 10.1039/C3EE43707H.
103. F. Matteocci, S. Razza, F. Di Giacomo, S. Casaluci, G. Mincuzzi, T. M. Brown, A. D'Epifanio, S. Licoccia and A. Di Carlo, *Phys. Chem. Chem. Phys.*, 2014, DOI: 10.1039/c3cp55313b.
104. A. Poglitsch and D. Weber, *The Journal of Chemical Physics*, 1987, 87, 6373-6378.
105. N. Onoda-Yamamuro, T. Matsuo and H. Suga, *Journal of Physics and Chemistry of Solids*, 1990, 51, 1383-1395.
106. H. Mashiyama, Y. Kawamura, E. Magome and Y. Kubota, *J Korean Phys Soc*, 2003, 42, S1026-S1029.
107. T. Leijtens, G. E. Eperon, S. Pathak, A. Abate, M. M. Lee and H. J. Snaith, *Nat Commun*, 2013, 4, DOI:10.1038/ncomms3885.

Biographies

Dr. Tze-Chien Sum is an Assistant Professor at the Division of Physics and Applied Physics, School of Physical and Mathematical Sciences, Nanyang Technological University (NTU) where he leads the Femtosecond Dynamics Laboratory. He received his Ph.D in 2005 from the National University of Singapore, where he worked on the development of a new direct-write lithographic technique (proton beam writing) for photonic applications. Upon joining NTU in 2005 as a Lecturer, he switched to the exciting field of ultrafast optical spectroscopy or Femtosecond time-resolved spectroscopy and established the *xC*-Lab research group – a lab for the investigation of e*xC*ited-state phenomena. His research focuses on investigating light matter interactions; energy and charge transfer mechanisms; and probing carrier and quasi-particle dynamics in a broad range of emergent nanoscale and light harvesting systems using Femtosecond time-resolved spectroscopy.

Dr. Nripan Mathews is an Assistant Professor at the School of Materials Engineering in Nanyang Technological University. He pursued his PhD at a joint Commissariat à l'énergie atomique (CEA) - Centre national de la recherche scientifique (CNRS) - Universite de Pierre et Marie Curie (Paris VI University) laboratory in the area of molecular crystals, studying the signatures of optical excitations within them (2008). He was also a visiting scientist at Prof. Michael Grätzel's laboratory at École Polytechnique Fédérale de Lausanne (EPFL), working on a pan-european project on photoelectrochemical hydrogen production. His research focuses on a wide variety of novel materials (metal oxides, organic semiconductors, graphene, carbon nanotubes, sulfides, selenides) and novel morphologies (One dimensional structures such as nanowires and nanotubes, thin films as well as two dimensional nanosheets) produced through a range of fabrication procedures. He has focussed primarily on the electronic and optical properties of these materials and how they can be adapted for practical applications.

TOC Graphical Abstract:

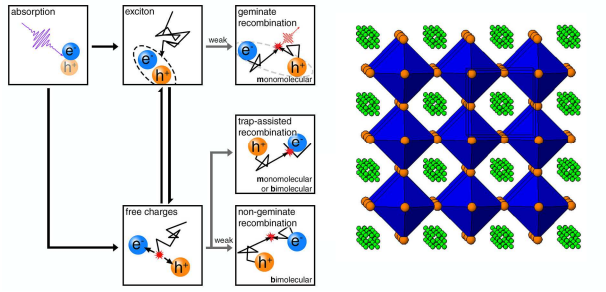

This article reviews the fundamental photophysics and working mechanisms of perovskite solar cells and highlights the current state-of-the-art and open questions in this maturing field.